Hindawi
Journal of Applied Mathematics
Volume 2019, Article ID 3084394, 19 pages
http://dx.doi.org/10.1155/2019/3084394

Research Article

A New Approximate Analytical Solutions for Two- and Three-Dimensional Unsteady Viscous Incompressible Flows by Using the Kinetically Reduced Local Navier-Stokes Equations

Abdul-Sattar J. Al-Saif and Assma J. Harfash

Department of Mathematics, College of Education for Pure Science, University of Basrah, Basrah, Iraq

Correspondence should be addressed to Assma J. Harfash; assmaj1974@yahoo.com

Received 13 October 2018; Accepted 9 December 2018; Published 1 January 2019

Academic Editor: Oluwole D. Makinde

In this work, the kinetically reduced local Navier-Stokes equations are applied to the simulation of two- and three-dimensional unsteady viscous incompressible flow problems. The reduced differential transform method is used to find the new approximate analytical solutions of these flow problems. The new technique has been tested by using four selected multidimensional unsteady flow problems: two- and three-dimensional Taylor decaying vortices flow, Kovasznay flow, and three-dimensional Beltrami flow. The convergence analysis was discussed for this approach. The numerical results obtained by this approach are compared with other results that are available in previous works. Our results show that this method is efficient to provide new approximate analytic solutions. Moreover, we found that it has highly precise solutions with good convergence, less time consuming, being easily implemented for high Reynolds numbers, and low Mach numbers.

1. Introduction

Many of the physical phenomena in fluid mechanics are formulated according to the unsteady viscous incompressible Navier-Stokes (INS) equations, which has the non-dimensional formula consisting of the momentum equations and the continuity equation [1–8]

$$\partial_t \mathbf{u} + (\mathbf{u} \cdot \nabla)\,\mathbf{u} + \nabla p = \frac{1}{Re}\nabla^2 \mathbf{u}, \tag{1}$$

$$\nabla \cdot \mathbf{u} = 0, \tag{2}$$

where t is the physical time, $\mathbf{u}$ is the velocity field, p is the pressure, and Re is the Reynolds number ($Re = \mathbb{U}L/\nu$, where $\mathbb{U}$ is the scale velocity field, L is the characteristic length, and ν is the kinematic viscosity of the fluid).

Analytical and numerical solutions of INS equations are known difficulty because they are non-linear equations, and they do not find the time evolution equation for the pressure that must be determined by solving the Passion equation at each time step, which requires effort and time. Therefore, there are a lot of studies that have developed an alternative formula description of incompressible fluid flows. One of these alternative formulas is the kinetically reduced local Navier-Stokes (KRLNS) equations which was suggested in [1] for the thermodynamic description of incompressible fluid flows at low Mach numbers. The system of KRLNS equations is

$$\partial_t \mathbf{u} + (\mathbf{u} \cdot \nabla)\,\mathbf{u} + \nabla p = \frac{1}{Re}\nabla^2 \mathbf{u}, \tag{3}$$

$$\partial_t g = -\frac{1}{(Ma)^2}\nabla \cdot \mathbf{u} + \frac{1}{Re}\nabla^2 g, \tag{4}$$

such that

$$p = g + \frac{\mathbf{u}^2}{2}, \tag{5}$$

where Ma is the Mach number ($Ma = \mathbb{U}/C_s$ is the ratio of the characteristic flow speed $\mathbb{U}$ to the isentropic sound speed C_s), and g is the grand potential. The time scale in INS equations related to that of KRLNS equations; $t_{KRLNS}(\tau) = Ma \times t_{NS}$.

All studies which have presented the KRLNS equations for simulation of unsteady incompressible viscous flow problems, used the numerical schemes for solving these equations. The KRLNS equations are proposed for the simulation of low Mach number flows in [2], and used the spectral element method to find the numerical solution of the three-dimensional Taylor Green vortex flow. In [3], two-dimensional KRLNS system is simplified and compared with a Chorin's artificial compressibility method for steady state computation of the flow in a lid-driven cavity at various Reynolds numbers, the Taylor Green vortex flow is demonstrated that the KRLNS equations correctly describe the time evolution of the velocity and of the pressure, for this purpose, the explicit Mac Cormack scheme is used. In [5] the KRLNS equations are applied to two-dimensional simulation of doubly periodic shear layers and decaying homogeneous isotropic turbulence, to solve these equations have been used the central difference scheme for the spatial discretization in both advection and diffusion terms and four stages Runge-Kutta method for the time integration, the numerical results are compared with those obtained by the artificial compressibility method, the lattice Boltzmann method, and the pseudospectral method. Higher order difference approximations are used in [6] to find the solutions of the KRLNS equations which are applied for two-dimensional simulations of Womersley problem and doubly periodic shear layers.

The main purpose of this paper is to find new approximate analytical solutions for two- and three-dimensional unsteady viscous incompressible flow problems. To achieve this objective, the flow problems that are described by alternative formulas of Navier-stokes equations, which are named KRLNS (3) and (4), the reduced differential transform method (RDTM) is proposed. The reasons that encourage us to propose RDTM to solve the present problems are being an effective and efficient method to find approximate analytical solutions for nonlinear equations and we believe that it has been achieved for the first time in its study. Moreover, we extend the application of RDTM and compare its reliability and efficiency with other methods. New approximate analytical solutions for two- and three-dimensional unsteady viscous incompressible flows were found using RDTM. The results that we obtained are better than others, refer to the results in [4, 8] in accuracy, convergence, and CPU time.

The structure of this paper is organized as follows: In Section 2, we begin with some basic definitions and the use of the RDTM on the KRLNS equations. Section 3 explains the manner we adopted to discuss the convergence of the solutions. In Section 4, we apply this method to solve four flow problems of different dimensions in order to show its ability and efficiency in finding new approximate solutions. Section 5 introduces conclusions of the present work.

2. Reduced Differential Transform Method

The RDTM is an iterative procedure for obtaining a Taylor series solution of differential equations. This method is similar to the differential transform method which was first introduced by Zhou [9]. RDTM has been successfully used to many nonlinear problems [10–19] since it does not require any parameter, discretization, linearization, or small perturbations; thus it reduces the size of computational work and is easily applicable.

The main idea of this method depends on the representation the function of two variables $u(x,t)$ as a product of single-variable function, i.e., $u(x,t) = f(x)g(t)$, then the function $u(x,t)$ can be represented as

$$u(x,t) = \sum_{i=0}^{\infty} F(i)\, x^i \sum_{j=0}^{\infty} G(j)\, t^j = \sum_{k=0}^{\infty} U_k(x)\, t^k, \tag{6}$$

Definition 1. If function $u(x,t)$ is analytic and differentiated continuously with respect to time t and space x, then

$$U_k(x) = \frac{1}{k!}\left[\frac{\partial^k}{\partial t^k} u(x,t)\right]_{t=0}, \tag{7}$$

is called t-dimensional spectrum function of $u(x,t)$, and is the transformed this function.

Definition 2. The reduced differential inverse transform of $U_k(x)$ is defined as

$$u(x,t) = \sum_{k=0}^{\infty} U_k(x)\, t^k. \tag{8}$$

Then, the inverse transformation of the set of $U_k(x)$ gives the $n-$terms approximation solution as follows:

$$u_n(x,t) = \sum_{k=0}^{n} U_k(x)\, t^k, \tag{9}$$

and the exact solution is

$$u(x,t) = \lim_{n\longrightarrow\infty} u_n(x,t). \tag{10}$$

To show some basic properties of $(n+1)$ dimensional RDTM [18], we have to consider $X = (x_1, x_2, \dots, x_n)$ to be a vector of n variables, and function $u(X,t)$ is analytic and continuously differentiable with respect to time t and space in the domain of interest, then the fundamental mathematical operations performed by RDTM are readily obtained and listed in Table 1.

For the application of this method with the KRLNS equations to find the approximate analytical solutions for INS equations, we referred to as (KRDTM) in this paper. In order to do that we suppose that $X = (x, y, z)$, $\mathbf{u} = (u, v, w)$, and $\mathbf{U}_k = (U_k, V_k, W_k)$, where $u(X,t)$, $v(X,t)$ and $w(X,t)$ are the fluid velocity components in the x, y, and z directions and $U_k(X)$, $V_k(X)$, $W_k(X)$, $G_k(X)$, and $P_k(X)$ are t-dimensional

Table 1: Reduced differential transformation.

Functional form	Transformed form
$w(X,t) = u(X,t) \pm v(X,t)$	$W_k(X) = U_k(X) \pm V_k(X)$
$w(X,t) = \alpha u(\dot{X},t)$	$W_k(X) = \alpha U_k(\dot{X})$, α is constant
$w(X,t) = u(X,t)v(\dot{X},t)$	$W_k(X) = \sum_{i=0}^{k} U_i(X)V_{k-i}(\dot{X})$
$w(X,t) = \dfrac{\partial^r}{\partial t^r}u(X,t)$	$W_k(X) = (k+1)\ldots(k+r)U_{k+r}(\dot{X}) = \dfrac{(k+r)!}{k!}U_{k+r}(\dot{X})$
$w(X,t) = \dfrac{\partial^{r_1+r_2\cdots+r_n}}{\partial x_1^{r_1}\partial x_2^{r_2}\ldots\partial x_n^{r_n}}u(X,t)$	$W_k(X) = \dfrac{\partial^{r_1+r_2\cdots+r_n}}{\partial x_1^{r_1}\partial x_2^{r_2}\ldots\partial x_n^{r_n}}U_k(X)$

spectrum functions of $u(X,t)$, $v(X,t)$, $w(X,t)$, $g(X,t)$, and $p(X,t)$, respectively, we get

$$(k+1)\mathbf{U}_{k+1}(X) = -\left(A_k + B_k + C_k + \nabla P_k(X)\right) + \frac{1}{Re}\nabla^2\mathbf{U}_k(X), \tag{11}$$

$$(k+1)G_{k+1}(X) = -\frac{1}{(Ma)^2}\nabla\cdot\mathbf{U}_k(X) + \frac{1}{Re}\nabla^2 G_k(X), \tag{12}$$

such that

$$\begin{aligned} P_k(X) &= G_k(X) + \frac{\mathbf{U}_k^2(X)}{2}, \\ A_k &= \sum_{i=0}^{k} U_i(X)\frac{\partial \mathbf{U}_{k-i}(X)}{\partial x}, \\ B_k &= \sum_{i=0}^{k} V_i(X)\frac{\partial \mathbf{U}_{k-i}(X)}{\partial y}, \\ C_k &= \sum_{i=0}^{k} W_i(X)\frac{\partial \mathbf{U}_{k-i}(X)}{\partial z}, \end{aligned} \tag{13}$$

where $k = 0,1,2,3,\ldots$, $U_0(X) = u(X,0)$, $V_0(X) = v(X,0)$, $W_0(X) = w(X,0)$, and $G_0(X) = g(X,0)$. Then the exact solution is obtained as follows:

$$\mathbf{u}(X,\tau) = \lim_{n\to\infty}\mathbf{u}_n(X,\tau), \tag{14}$$

where

$$\mathbf{u}_n(X,\tau) = \sum_{k=0}^{n}\mathbf{U}_k(X)\tau^k. \tag{15}$$

3. Analysis of Convergence

The convergence of the approximate analytical solutions that are resulted from the application of RDTM to INS equations is discussed by relying on the approach followed in [20, 21].

Let us consider the Hilbert space $H = L^2((a,b)^3 \times [0,T])$ define by

$$u : H \longrightarrow \mathbb{R} \text{ with } \int_{(a,b)^3\times[0,T]} u^2(X,t)\,dX\,dt < \infty, \tag{16}$$

and the norm $\|u\|^2 = \int_{(a,b)^3\times[0,T]} u^2(X,t)\,dX\,dt$. Define

$$\mathbf{u} = (u,v,w) : H^3 \longrightarrow \mathbb{R}^3 \text{with} \int_{(a,b)^3\times[0,T]} \left(u^2(X,t) + v^2(X,t) + w^2(X,t)\right)dX\,dt < \infty, \tag{17}$$

such that $\|\mathbf{u}\|^2 = \|u\|^2 + \|v\|^2 + \|w\|^2$.

We consider the INS equation in the following form:

$$\mathscr{L}(\mathbf{u}(X,t)) = \mathscr{N}(\mathbf{u}(X,t)) + \mathscr{R}(\mathbf{u}(X,t)), \tag{18}$$

which is equivalent to the following form:

$$\mathbf{u}(X,t) = \mathscr{F}\left(\mathbf{u}_k(X,t)\right), \tag{19}$$

where $\mathscr{L} = \partial_t$ is the linear partial derivative with respect to t, $\mathscr{N}$ is a nonlinear operator, $\mathscr{R}$ is a linear operator, and $\mathscr{F}$ is a general nonlinear operator involving both linear and nonlinear terms. According to RDTM

$$(k+1)\mathbf{U}_{k+1}(X) = \mathscr{N}\left(\mathbf{U}_k(X)\right) + \mathscr{R}\left(\mathbf{U}_k(X)\right), \tag{20}$$

and the solutions

$$\mathbf{u}(X,t) = \sum_{k=0}^{\infty}\mathbf{U}_k(X)t^k = \sum_{k=0}^{\infty}\mathscr{B}_k, \tag{21}$$

where $\mathscr{B}_k = (\mathscr{B}_{1k}, \mathscr{B}_{2k}, \mathscr{B}_{3k})$. It is noted that the solutions by RDTM are equivalent to determining the sequence

$$\begin{aligned} \mathbf{S}_0 &= \mathbf{U}_0(X) = \mathscr{B}_0, \\ \mathbf{S}_1 &= \mathbf{U}_0(X) + \mathbf{U}_1(X)t = \mathscr{B}_0 + \mathscr{B}_1, \\ \mathbf{S}_2 &= \mathbf{U}_0(X) + \mathbf{U}_1(X)t + \mathbf{U}_2(X)t^2 = \mathscr{B}_0 + \mathscr{B}_1 + \mathscr{B}_2, \\ &\vdots \\ \mathbf{S}_n &= \sum_{k=0}^{n}\mathbf{U}_k(X)t^k = \sum_{k=0}^{n}\mathscr{B}_k, \end{aligned} \tag{22}$$

such that $\mathbf{S}_{n+1} = \mathscr{F}(\mathbf{S}_n)$.

The sufficient condition for convergence of the series solution $\{\mathbf{S}_n\}_0^\infty$ is presented in the following theorems

Theorem 3. *The series solution $\{\mathbf{S}_n = (R_n, S_n, T_n)\}_0^\infty$ converges whenever there is γ such that $0 < \gamma < 1$, $\gamma = \gamma_1 + \gamma_2 + \gamma_3$, and $\|\mathscr{B}_{i(k+1)}\| \leqslant \gamma_i\|\mathscr{B}_{ik}\|$*

Proof. We show that $\{\mathbf{S}_n = (R_n, S_n, T_n)\}_0^\infty$ is a Cauchy sequence in the Hilbert space H^3. For this reason, consider

$$\begin{aligned}
\|R_{n+1} - R_n\| &= \|\mathscr{B}_{1(n+1)}\| \leqslant \gamma_1 \|\mathscr{B}_{1n}\| \leqslant \gamma_1^2 \|\mathscr{B}_{1(n-1)}\| \\
&\leqslant \cdots \leqslant \gamma_1^{n+1} \|\mathscr{B}_{10}\|, \\
\|S_{n+1} - S_n\| &= \|\mathscr{B}_{2(n+1)}\| \leqslant \gamma_2 \|\mathscr{B}_{2n}\| \leqslant \gamma_2^2 \|\mathscr{B}_{2(n-1)}\| \\
&\leqslant \cdots \leqslant \gamma_2^{n+1} \|\mathscr{B}_{20}\|, \\
\|T_{n+1} - T_n\| &= \|\mathscr{B}_{3(n+1)}\| \leqslant \gamma_3 \|\mathscr{B}_{3n}\| \leqslant \gamma_3^2 \|\mathscr{B}_{3(n-1)}\| \\
&\leqslant \cdots \leqslant \gamma_3^{n+1} \|\mathscr{B}_{30}\|,
\end{aligned} \tag{23}$$

Using triangle inequality

$$\begin{aligned}
&\|\mathbf{S}_n - \mathbf{S}_m\| = \|(R_n, S_n, T_n) - (R_m, S_m, T_m)\| \\
&\quad = \|(R_n - R_m, S_n - S_m, T_n - T_m)\| \leqslant \|R_n - R_m\| \\
&\quad + \|S_n - S_m\| + \|T_n - T_m\| \leqslant \|R_n - R_{n-1}\| \\
&\quad + \|R_{n-1} - R_{n-2}\| + \cdots + \|R_{m+1} - R_m\| \\
&\quad + \|S_n - S_{n-1}\| + \|S_{n-1} - S_{n-2}\| + \cdots + \|S_{m+1} - S_m\| \\
&\quad + \|T_n - T_{n-1}\| + \|T_{n-1} - T_{n-2}\| + \cdots + \|T_{m+1} - T_m\| \\
&\quad \leqslant \left(\gamma_1^n + \gamma_1^{n-1} + \cdots + \gamma_1^{m+1}\right) \|\mathscr{B}_{10}\| \\
&\quad + \left(\gamma_2^n + \gamma_2^{n-1} + \cdots + \gamma_2^{m+1}\right) \|\mathscr{B}_{20}\| \\
&\quad + \left(\gamma_3^n + \gamma_3^{n-1} + \cdots + \gamma_3^{m+1}\right) \|\mathscr{B}_{30}\| \\
&\quad \leqslant \left(\gamma^n + \gamma^{n-1} + \cdots + \gamma^{m+1}\right) \\
&\quad \cdot \left(\|\mathscr{B}_{10}\| + \|\mathscr{B}_{20}\| + \|\mathscr{B}_{30}\|\right) \\
&\quad = \gamma^{m+1} \left(\gamma^{n-m-1} + \gamma^{n-m-2} + \cdots + 1\right) \\
&\quad \cdot \left(\|\mathscr{B}_{10}\| + \|\mathscr{B}_{20}\| + \|\mathscr{B}_{30}\|\right) \leqslant \frac{\gamma^{m+1}}{1-\gamma} \|\mathscr{B}_0\|
\end{aligned} \tag{24}$$

since $\|\mathscr{B}_0\| < \infty$ and $0 < \gamma < 1$, we get $\lim_{n,m \to \infty} \|\mathbf{S}_n - \mathbf{S}_m\| = 0$; thus, we conclude that $\{\mathbf{S}_n\}_0^\infty$ is a Cauchy sequence in the Hilbert space H^3, then the series solution $\{\mathbf{S}_n\}_0^\infty$ converges to some $\{\mathbf{S}\} \in H^3$. □

Theorem 4. *Let $\mathscr{F} = (\mathscr{F}_1, \mathscr{F}_2, \mathscr{F}_3)$ be a nonlinear operator satisfies Lipschitz condition from a Hilbert space H^3 into H^3 and $\mathbf{u}(X, t)$ be the exact solution of INS equations. If the series solution $\{\mathbf{S}_n\}_0^\infty$ converges, then it is converged to $\mathbf{u}(X, t)$.*

Proof. Let $\mathbf{u}_1(X, t), \mathbf{u}_2(X, t)$, and we have

$$\begin{aligned}
&\|\mathscr{F}(\mathbf{u}_1) - \mathscr{F}(\mathbf{u}_2)\| = \|(\mathscr{F}_1(\mathbf{u}_1), \mathscr{F}_2(\mathbf{u}_1), \mathscr{F}_3(\mathbf{u}_1)) \\
&\quad - (\mathscr{F}_1(\mathbf{u}_2), \mathscr{F}_2(\mathbf{u}_2), \mathscr{F}_3(\mathbf{u}_2))\| = \|(\mathscr{F}_1(\mathbf{u}_1) \\
&\quad - \mathscr{F}_1(\mathbf{u}_2), \mathscr{F}_2(\mathbf{u}_1) - \mathscr{F}_2(\mathbf{u}_2), \mathscr{F}_3(\mathbf{u}_1) \\
&\quad - \mathscr{F}_3(\mathbf{u}_2))\| \leqslant \|\mathscr{F}_1(\mathbf{u}_1) - \mathscr{F}_1(\mathbf{u}_2)\| + \|\mathscr{F}_2(\mathbf{u}_1) \\
&\quad - \mathscr{F}_2(\mathbf{u}_2)\| + \|\mathscr{F}_3(\mathbf{u}_1) - \mathscr{F}_3(\mathbf{u}_2)\| \leqslant \gamma_1 \|\mathbf{u}_1 - \mathbf{u}_2\| \\
&\quad + \gamma_2 \|\mathbf{u}_1 - \mathbf{u}_2\| + \gamma_3 \|\mathbf{u}_1 - \mathbf{u}_2\| = (\gamma_1 + \gamma_2 + \gamma_3) \|\mathbf{u}_1 \\
&\quad - \mathbf{u}_2\| = \gamma \|\mathbf{u}_1 - \mathbf{u}_2\|.
\end{aligned} \tag{25}$$

Therefore, there is a unique solution of the problem (18) by the Banach fixed-point theorem. Now we should prove that $\{\mathbf{S}_n\}_0^\infty$ converges to $\mathbf{u}(X, t)$

$$\begin{aligned}
\mathbf{u}(X, t) &= \mathscr{F}(\mathbf{u}(X, t)) = \mathscr{F}\left(\sum_{k=0}^{\infty} \mathscr{B}_k\right) \\
&= \mathscr{F}\left(\lim_{n \to \infty} \sum_{k=0}^{n} \mathscr{B}_k\right) = \lim_{n \to \infty} \mathscr{F}\left(\sum_{k=0}^{n} \mathscr{B}_k\right) \\
&= \lim_{n \to \infty} \mathscr{F}(\mathbf{S}_n) = \lim_{n \to \infty} \mathbf{S}_{n+1} = \mathbf{S}.
\end{aligned} \tag{26}$$

□

Definition 5. For $i = 1, 2, 3$ and $k \in \mathbb{N} \bigcup \{0\}$, we define

$$\gamma_{ik} = \begin{cases} \dfrac{\|\mathscr{B}_{i(k+1)}\|}{\|\mathscr{B}_{ik}\|}, & \|\mathscr{B}_{ik}\| \neq 0, \\ 0, & \|\mathscr{B}_{ik}\| = 0. \end{cases} \tag{27}$$

then we can say that $\sum_{k=0}^{\infty} \mathbf{U}_k(X) t^k$ converges to the exact solution $\mathbf{u}(X, t)$ when $\gamma_k = \gamma_{1k} + \gamma_{2k} + \gamma_{3k}$ and $0 < \gamma_k < 1$ for all $k \in \mathbb{N} \bigcup \{0\}$.

4. Test Problems

In this section, the KRDTM is applied to find approximate analytical solutions of four unsteady viscous incompressible flow problems, two of these problems have exact solutions and the others do not have the exact solutions. We applied KRDTM for each problem to get some approximate analytical solutions. Then the convergence of these solutions has been discussed theoretically and numerically. Finally, the results have been reviewed through some figures, which represent the velocity components and the vorticity functions, which satisfy

$$\Omega = \nabla \times \mathbf{u}, \tag{28}$$

and explain the time development with the enstrophy, which is defined as

$$\varepsilon = \frac{1}{2V} \int_V \Omega^2 dV, \tag{29}$$

where V is volume for three-dimension flow problems. Our results are computed by using various value of Reynolds numbers at some time levels. All our calculations are run by Maple 18 software.

First problem (P1) is two-dimensional Taylor decaying vortices flow [4, 7, 8], which describes an initially periodical vortex structure convected by the flow field and exponentially decaying due to the viscous decaying. The exact solution of this problem that achieves (1) and (2) is

$$\begin{aligned} u(x,y,t) &= -\cos(x)\sin(y)\,e^{-2t/Re},\\ v(x,y,t) &= \sin(x)\cos(y)\,e^{-2t/Re},\\ p(x,y,t) &= -\frac{1}{4}\left(\cos(2x)+\cos(2y)\right)e^{-4t/Re}, \end{aligned} \tag{30}$$

when we used KRDTM for solving two-dimensional (1) and (2) equations, where $X=(x,y)$, $\mathbf{u}=(u,v)$, $\mathbf{U}_k=(U_k,V_k)$, and $t_{KRLNS}:=\tau$; we get

$$\begin{aligned} &(k+1)\,U_{k+1}(x,y)\\ &\quad = -\left(A1_k + B1_k + \frac{\partial P_k(x,y)}{\partial x}\right)\\ &\qquad + \frac{1}{Re}\left(\frac{\partial^2 U_k(x,y)}{\partial x^2} + \frac{\partial^2 U_k(x,y)}{\partial y^2}\right), \end{aligned} \tag{31}$$

$$\begin{aligned} &(k+1)\,V_{k+1}(x,y)\\ &\quad = -\left(A2_k + B2_k + \frac{\partial P_k(x,y)}{\partial y}\right)\\ &\qquad + \frac{1}{Re}\left(\frac{\partial^2 V_k(x,y)}{\partial x^2} + \frac{\partial^2 V_k(x,y)}{\partial y^2}\right), \end{aligned} \tag{32}$$

$$\begin{aligned} &(k+1)\,G_{k+1}(x,y)\\ &\quad = -\frac{1}{(Ma)^2}\left(\frac{\partial U_k(x,y)}{\partial x} + \frac{\partial V_k(x,y)}{\partial y}\right)\\ &\qquad + \frac{1}{Re}\left(\frac{\partial^2 G_k(x,y)}{\partial x^2} + \frac{\partial^2 G_k(x,y)}{\partial y^2}\right), \end{aligned} \tag{33}$$

such that

$$\begin{aligned} P_k(x,y) &= G_k(x,y) + \frac{U_k^2(x,y)+V_k^2(x,y)}{2},\\ A1_k &= \sum_{i=0}^{k} U_i(x,y)\,\frac{\partial U_{k-i}(x,y)}{\partial x},\\ B1_k &= \sum_{i=0}^{k} V_i(x,y)\,\frac{\partial U_{k-i}(x,y)}{\partial y},\\ A2_k &= \sum_{i=0}^{k} U_i(x,y)\,\frac{\partial V_{k-i}(x,y)}{\partial x},\\ B2_k &= \sum_{i=0}^{k} V_i(x,y)\,\frac{\partial V_{k-i}(x,y)}{\partial y}, \end{aligned} \tag{34}$$

where $k=0,1,2,3,\ldots$, $U_0(x,y)=u(x,y,0)$, $V_0(x,y)=v(x,y,0)$, and $G_0(x,y)=g(x,y,0)$; the solutions are produced as follows:

$$u(x,y,\tau) = \lim_{n\longrightarrow\infty} u_n(x,y,\tau), \tag{35}$$

$$v(x,y,\tau) = \lim_{n\longrightarrow\infty} v_n(x,y,\tau), \tag{36}$$

$$g(x,y,\tau) = \lim_{n\longrightarrow\infty} g_n(x,y,\tau), \tag{37}$$

where

$$\begin{aligned} u_n(x,y,\tau) &= \sum_{k=0}^{n} U_k(x,y)\,\tau^k,\\ v_n(x,y,\tau) &= \sum_{k=0}^{n} V_k(x,y)\,\tau^k,\\ g_n(x,y,\tau) &= \sum_{k=0}^{n} G_k(x,y)\,\tau^k, \end{aligned} \tag{38}$$

such that

$$\begin{aligned} U_1(x,y) &= \frac{2}{Re}\cos(x)\sin(y),\\ U_2(x,y) &= -\frac{2}{(Re)^2}\cos(x)\sin(y)\\ &\quad - \frac{2}{Re}\sin(2x)\cos(2y),\\ &\vdots,\\ V_1(x,y) &= -\frac{2}{Re}\sin(x)\cos(y),\\ V_2(x,y) &= \frac{2}{(Re)^2}\sin(x)\cos(y)\\ &\quad - \frac{2}{Re}\cos(2x)\sin(2y),\\ &\vdots, \end{aligned} \tag{39}$$

and

$$\begin{aligned} G_1(x,y) &= \frac{1}{Re}\left(\cos(2x)+\cos(2y)\right)\\ &\quad + \frac{2}{Re}\left(\cos^2(x)\sin^2(y) - \sin^2(x)\sin^2(y)\right.\\ &\quad \left. - \cos^2(y)\cos^2(x) + \cos^2(y)\sin^2(x)\right),\\ G_2(x,y) &= -\frac{2}{(Re)^2}\left(\cos(2x)+\cos(2y)\right)\\ &\quad - \frac{8}{(Re)^2}\left(\cos^2(x)\sin^2(y) - \sin^2(x)\sin^2(y)\right.\\ &\quad \left. - \cos^2(y)\cos^2(x) + \cos^2(y)\sin^2(x)\right),\\ &\vdots \end{aligned} \tag{40}$$

To prove that the condition of the convergence of these solutions verified on the domain $[0, 2\pi]^2$ apply Definition 5

$$\gamma_{10} = \frac{\|U_1(x, y)\tau\|}{\|U_0(x, y)\|} = \frac{2\tau}{Re},$$
$$\gamma_{20} = \frac{\|V_1(x, y)\tau\|}{\|V_0(x, y)\|} = \frac{2\tau}{Re},$$
$$\gamma_{30} = \frac{\|G_1(x, y)\tau\|}{\|G_0(x, y)\|} = \frac{3.771236166\tau}{Re},$$
$$\gamma_{11} = \frac{\|U_2(x, y)\tau^2\|}{\|U_1(x, y)\tau\|} = \frac{\sqrt{(Re)^2 + 4\tau}}{2Re}, \tag{41}$$
$$\gamma_{21} = \frac{\|V_2(x, y)\tau^2\|}{\|V_1(x, y)\tau\|} = \frac{\sqrt{(Re)^2 + 4\tau}}{2Re},$$
$$\gamma_{31} = \frac{\|G_2(x, y)\tau^2\|}{\|G_1(x, y)\tau\|} = \frac{3.162277660\tau}{2Re},$$
$$\vdots,$$

such that $\gamma_0 = \gamma_{10} + \gamma_{20} + +\gamma_{30}, \gamma_1 = \gamma_{11} + \gamma_{21} + \gamma_{31}, \ldots$. For example, if $t = 0.5$, $Ma = 0.001$, and $Re = 100$ such that $\tau = Ma \times t$, for all x and y in this domain, then

$$\gamma_0 = 0.3885618083 \times 10^{-4} < 1,$$
$$\gamma_1 = 0.5159113783 \times 10^{-3} < 1, \ldots \tag{42}$$

and if $Re = 1000$ then

$$\gamma_0 = 3.885618083 \times 10^{-6} < 1,$$
$$\gamma_1 = 0.5015821387 \times 10^{-3} < 1, \ldots \tag{43}$$

if $t = 2$ and $Re = 100$ then

$$\gamma_0 = 0.1554247233 \times 10^{-3} < 1,$$
$$\gamma_1 = 0.2063645515 \times 10^{-2} < 1, \ldots \tag{44}$$

and if $Re = 1000$ then

$$\gamma_0 = 0.1554247233 \times 10^{-4} < 1,$$
$$\gamma_1 = 0.2006328556 \times 10^{-2} < 1, \ldots \tag{45}$$

The errors measurements L_1, L_2, and L_∞-norm resulting from the application of KRDTM and the implicit central compact method (ICCM) in [8] for the computed u velocity component with CPU time for various grids at time level $t = 0.5$, $Ma = 0.001$, and $Re = 100$ are tabulated in Table 2. In Table 3, L_2-norm errors for u are calculated at time level $t = 5$ and $Ma = 0.001$ for various Reynolds numbers. The contours of the vorticity and pressure are explained in Figure 1 at $t = 2$, $Ma = 0.01$, and $Re = 100$. The comparisons of the computed u and v velocity components with the exact solution along the vertical and horizontal center lines at time levels $t = 2$, $Ma = 0.01$, and $Re = 100$ are shown in Figure 2. In Table 2, it can be noticed that the accuracy of new solutions and the size of the calculated errors of KRDTM are not often affected by the grid size which has been used in comparison with numerical results. Moreover, the results of KRDTM are better than ICCM [8]. Also, from this table, it is clearly shown that the KRDTM results in less computation time (CPU) than ICCM [8]. In Table 3, the same facts have been shown with various Reynolds numbers and grid spacing for L_2-norm at $t = 5$, where in some cases the CPU time reached zero. The results are given in Figure 1 show that the profiles of vorticity and pressure as contour plot are equivalent and identical with other results in [4, 7, 8]. Moreover Figure 2 compares between the exact and new approximate analytical solutions, and the identical is confirmation of the efficiency of KRDTM in solving INS equations with good convergence for different time.

Second problem (P2) is Kovasznay flow [4, 7, 8], which is the laminar flow of viscous fluid behind a two-dimensional grid, with x-axis normal to the grid and the velocity field is assumed to be such that $u := \mathbb{U} + u$ and $v := v$, where $u(x, y, t)$ and $v(x, y, t)$ are the components of velocity; $\mathbb{U}$ is the average velocity in the x-direction. Thus, the two-dimensional INS equations with a periodicity in one direction may represent the wake of a two-dimensional grid the same as (1) with replacing the convective terms by $((\mathbb{U}+u, v)\cdot\nabla)(u, v)$, where $\mathbb{U}$ refers to one in this test. When we solved two-dimensional equations (1) and (2) by using KRDTM for this test problem, we get the same equations (31), (32), and (33) with

$$A_k = \frac{\partial U_k(x, y)}{\partial x} + \sum_{i=0}^{k} U_i(x, y) \frac{\partial U_{k-i}(x, y)}{\partial x},$$
$$B_k = \sum_{i=0}^{k} V_i(x, y) \frac{\partial U_{k-i}(x, y)}{\partial y},$$
$$D_k = \frac{\partial V_k(x, y)}{\partial x} + \sum_{i=0}^{k} U_i(x, y) \frac{\partial V_{k-i}(x, y)}{\partial x}, \tag{46}$$
$$E_k = \sum_{i=0}^{k} V_i(x, y) \frac{\partial V_{k-i}(x, y)}{\partial y}.$$

The exact solution of the steady state of this problem [7] considers the initial conditions in this test

$$u(x, y, 0) = 1 - e^{\lambda x} \cos(2\pi y),$$
$$v(x, y, 0) = \frac{\lambda}{2\pi} e^{\lambda x} \sin(2\pi y), \tag{47}$$
$$p(x, y, 0) = p_0 - \frac{1}{2} e^{2\lambda x},$$

Table 2: The L_1, L_2, and L_∞-norm errors for u of **P1** at $t = 0.5$ and $Ma = 0.001$.

Grid size	method	L_1-norm	L_2-norm	L_∞-norm	CPUs
11×11	KRDTM	3.34×10^{-8}	5.82×10^{-9}	1.19×10^{-9}	0.062
	ICCM [8]	3.56×10^{-2}	4.24×10^{-2}	7.37×10^{-2}	6.83
21×21	KRDTM	3.19×10^{-8}	5.69×10^{-9}	1.19×10^{-9}	0.172
	ICCM [8]	4.71×10^{-4}	5.73×10^{-4}	1.09×10^{-3}	27.81
41×41	KRDTM	3.15×10^{-8}	5.62×10^{-9}	1.91×10^{-9}	0.967
	ICCM [8]	7.15×10^{-6}	8.72×10^{-6}	1.69×10^{-5}	107.45
81×81	KRDTM	3.15×10^{-8}	5.59×10^{-9}	1.91×10^{-9}	2.57
	ICCM [8]	1.67×10^{-7}	2.05×10^{-7}	4.01×10^{-7}	432.14
161×161	KRDTM	3.15×10^{-8}	5.57×10^{-9}	1.91×10^{-9}	10.8
	ICCM [8]	3.64×10^{-8}	4.45×10^{-8}	8.71×10^{-8}	1770.30

Table 3: The L_2-norm errors for u of **P1** at $t = 5$ and $Ma = 0.001$.

Grid size	Re=40	Re=100	Re=500	Re=1000	Max CPUs
11×11	1.46×10^{-6}	5.82×10^{-7}	1.16×10^{-7}	5.82×10^{-8}	0
21×21	1.42×10^{-6}	5.69×10^{-7}	1.14×10^{-7}	5.69×10^{-8}	0.016
41×41	1.40×10^{-6}	5.62×10^{-7}	1.12×10^{-7}	5.62×10^{-8}	0.047
81×81	1.40×10^{-6}	5.59×10^{-7}	1.12×10^{-7}	5.59×10^{-8}	0.172
161×161	1.39×10^{-6}	5.57×10^{-7}	1.11×10^{-7}	5.57×10^{-8}	0.655
321×321	1.39×10^{-6}	5.56×10^{-7}	1.11×10^{-7}	5.56×10^{-8}	2.53

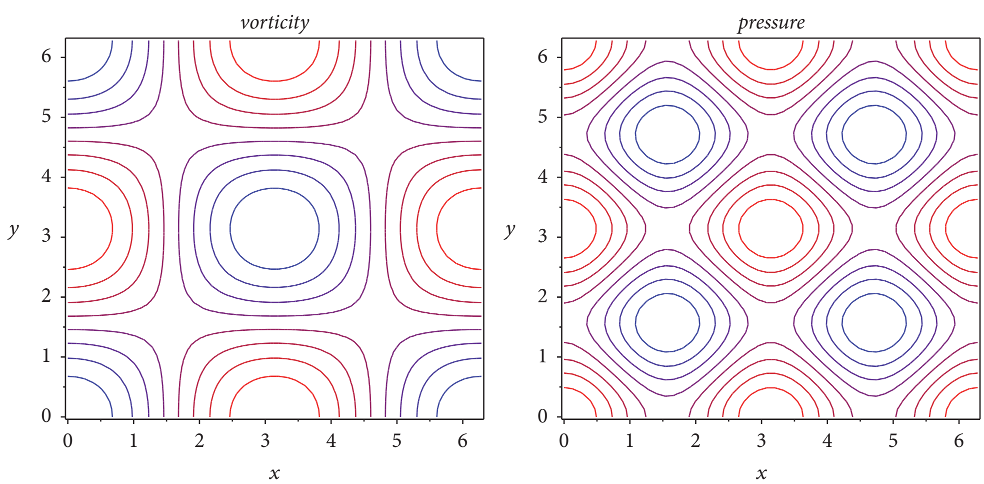

Figure 1: Contours plots of vorticity and pressure of **P1**.

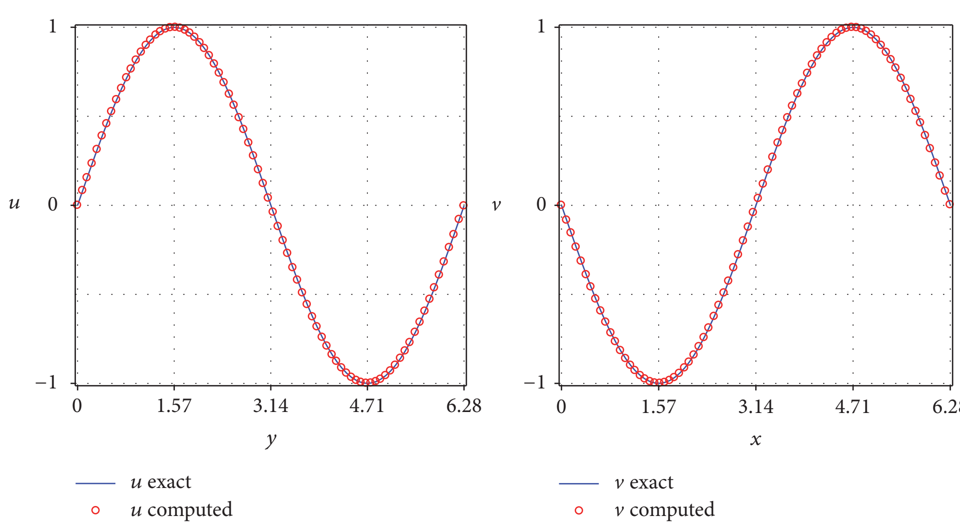

Figure 2: The comparison of the computed $u(\pi, y)$ and $v(x, \pi)$ with the exact solutions of **P1**.

where $\lambda = Re/2 - \sqrt{(Re)^2 + 16\pi^2}/2$, p_0 is a reference pressure (an arbitrary constant), and $p_0 = 0$ in the test. The solutions produce similar solutions in (35), (36), and (37) with

$$\begin{aligned}
U_1(x,y) &= e^{x\lambda}\cos(2\pi y)\left(\frac{4\pi^2-\lambda^2}{Re}+2\lambda\right),\\
U_2(x,y) &= -\frac{1}{2}e^{x\lambda}\cos(2\pi y)\left(\frac{4\pi^2-\lambda^2}{Re}+2\lambda\right)^2\\
&\quad+\left(2\lambda e^{2x\lambda}-\frac{1}{2}e^{x\lambda}\cos(2\pi y)\right.\\
&\quad\left.-\frac{\lambda(4\pi^2-\lambda^2)}{4\pi^2}e^{2x\lambda}\sin^2(2\pi y)\right)\\
&\quad-\frac{\lambda}{2Re}\left[8(2\pi^2-\lambda^2)e^{2x\lambda}\cos^2(2\pi y)\right.\\
&\quad-(4\pi^2-\lambda^2)e^{x\lambda}\cos(2\pi y)-2(4\pi^2+\lambda^2)e^{2x\lambda}\\
&\quad\left.-\frac{\lambda^4}{\pi^2}e^{x\lambda}\sin^2(2\pi y)\right],\\
&\ \ \vdots,
\end{aligned}\tag{48}$$

$$\begin{aligned}
V_1(x,y) &= -\frac{\lambda}{2\pi}e^{x\lambda}\sin(2\pi y)\left(\frac{4\pi^2-\lambda^2}{Re}+2\lambda\right),\\
V_2(x,y) &= \frac{\lambda}{2\pi}e^{x\lambda}\sin(2\pi y)\left(\frac{4\pi^2-\lambda^2}{Re}+2\lambda\right)^2\\
&\quad+\frac{e^{x\lambda}}{4\pi}\sin(2\pi y)\left((4\pi^2+\lambda^2)\right.\\
&\quad\left.-2\cos(2\pi y)(4\pi^2-\lambda^2)\right)\left(\frac{4\pi^2-\lambda^2}{Re}+2\lambda\right)\\
&\quad-\frac{4\pi^2-\lambda^2}{2\pi Re}e^{x\lambda}\sin(2\pi y)\left(\pi^2\right.\\
&\quad\left.-e^{x\lambda}\cos(2\pi y)(4\pi^2-\lambda^2)\right),\\
&\ \ \vdots,
\end{aligned}$$

and

$$\begin{aligned}
G_1(x,y) &= \frac{e^{x\lambda}}{Re}\left[\left(4(2\pi^2-\lambda^2)\cos^2(2\pi y)\right.\right.\\
&\quad\left.-(4\pi^2+\lambda^2)-\frac{\lambda^4}{2\pi^2}\sin^2(2\pi y)\right)e^{x\lambda}-(4\pi^2-\lambda^2)\\
&\quad\left.\cdot\cos(2\pi y)\right],\\
G_2(x,y) &= \frac{e^{x\lambda}}{\pi^2(Re)^2}\left[\left(\lambda^6-12\lambda^4\pi^2+48\lambda^2\pi^4\right.\right.\\
&\quad\left.-64\pi^6\right)e^{x\lambda}\cos(2\pi y)+\left(0.5\lambda^4\pi^2-4\lambda^2\pi^4+8\pi^6\right)\\
&\quad\left.\cdot\cos^2(2\pi y)-\left(\lambda^6+24\lambda^2\pi^4-32\pi^6\right)e^{x\lambda}\right],\\
&\ \ \vdots
\end{aligned}\tag{49}$$

These solutions satisfy the conditions of convergence in the domain $[-0.5, 1.5]^2$,

$$\begin{aligned}
\gamma_{10} &= \frac{\|U_1(x,y)\tau\|}{\|U_0(x,y)\|}\\
&= \sqrt{\frac{(\lambda^2-39.47841760-2\lambda Re)^2(e^{3\lambda}-e^{-\lambda})\tau^2}{2(Re)^2(8\lambda+e^{3\lambda}-e^{-\lambda})}},\\
\gamma_{20} &= \frac{\|V_1(x,y)\tau\|}{\|V_0(x,y)\|}\\
&= \sqrt{\frac{(\lambda^2-39.47841760-2\lambda Re)^2\tau^2}{(Re)^2}},\\
\gamma_{30} &= \frac{\|G_1(x,y)\tau\|}{\|G_0(x,y)\|} = 2\left[\frac{\tau^2}{(Re)^2}\left((e^{8\lambda}-1)\left(0.5625\lambda^8\right.\right.\right.\\
&\quad+59.21762641\lambda^6+7013.454554\lambda^4\\
&\quad\left.-46146.68129\lambda^2+455449.4888\right)+\left(e^{4\lambda}-1\right)\\
&\quad\cdot e^{\lambda}\left(584.4545462\lambda^4-46146.68129\lambda^2\right.\\
&\quad\left.\left.\left.+910898.9775\right)\right)\right]^{1/2}\div\left[\left(e^{8\lambda}-1\right)\left(0.140625\lambda^4\right.\right.\\
&\quad\left.+18.50550825\lambda^2+1388.079547\right)+e^{\lambda}\left(e^{4\lambda}-1\right)\\
&\quad\cdot\left(29.60881320\lambda^2+5844.545462\right)\\
&\quad\left.+4675.636370\lambda e^{2\lambda}\right]^{1/2},\\
&\ \ \vdots
\end{aligned}\tag{50}$$

For example, if $Ma = 0.01$, $t = 0.1$ such that $\tau = Ma \times t$, and $Re = 20$, for all x and y, then

$$\begin{aligned}
\gamma_0 &= 0.417945328\times10^{-2} < 1,\\
\gamma_1 &= 0.6772122966\times10^{-1} < 1,\ldots
\end{aligned}\tag{51}$$

if $Re = 40$ then

$$\begin{aligned}
\gamma_0 &= 0.2106111743\times10^{-2} < 1,\\
\gamma_1 &= 0.8546834826\times10^{-1} < 1,\ldots
\end{aligned}\tag{52}$$

and if $Re = 100$ then

$$\gamma_0 = 0.8607760699 \times 10^{-3} < 1,$$
$$\gamma_1 = 0.1755994678 < 1, \ldots \tag{53}$$

In Tables 4 and 5, the L_2-norm error for the computed velocity component at $Ma = 0.01$ for some values of Reynolds numbers is compared with the numerical results of the upwind compact finite difference method (UCFDM) in [4]. We noticed that the accuracy of the results obtained from KRDTM is higher and better than the results of UCFDM for different values of Reynolds numbers. It is clear that the maximum CPU time for all cases is not more than 30.0s, and iterations number (3) of KRDTM is less than iterations number of UCFDM (number of iterations $\leqslant$ 3000). This shows that KRDTM is faster convergence and more accurate than UCFDM. The influence of the Reynolds number value on the computed vorticity and stream function $\psi(x, y, t)$ which is satisfied

$$\partial_y \psi(x, y, t) = u(x, y, t),$$
$$\partial_x \psi(x, y, t) = -v(x, y, t) \tag{54}$$

is explained in Figure 3, so that the pairs of bound eddies produced behind the single elements of the grids and at large distance downstream. However, the streamlines are parallel and equidistant as shown by the short lines on the right side of the figure for all values of Reynolds numbers. We also note that when the value of Reynolds number increases, the whole flow pattern is expanded uniformly in the direction of main flow. Moreover, it can be observed that the rate of change of the flow is very great, and the length of vortices increases towards the downstream flow with the increase in the Reynolds number.

Third problem (P3) is three-dimensional Taylor decaying vortices flow, whose initial conditions [22–26] are given by

$$\begin{aligned}
u(x, y, z, 0) &= \mathbb{U} \sin\left(\frac{x}{L}\right) \cos\left(\frac{y}{L}\right) \cos\left(\frac{z}{L}\right), \\
v(x, y, z, 0) &= -\mathbb{U} \cos\left(\frac{x}{L}\right) \sin\left(\frac{y}{L}\right) \cos\left(\frac{z}{L}\right), \\
w(x, y, z, 0) &= 0, \\
p(x, y, z, 0) &= p_0 + \frac{\rho_0 \mathbb{U}^2}{16} \left(\cos\left(\frac{2x}{L}\right) + \cos\left(\frac{2y}{L}\right)\right) \\
&\quad \cdot \left(\cos\left(\frac{2z}{L}\right) + 2\right),
\end{aligned} \tag{55}$$

with periodic boundary conditions in all directions, where p_0 is a reference pressure (an arbitrary constant), $\mathbb{U}$ is characteristic velocity, ρ_0 is the density, and L is the inverse of the wave number of the minimum frequencies (the largest length scale of flow). We used in this test $p_0 = 0$, $\mathbb{U} = 1$, $\rho_0 = 1$, and $L = 1$ [23] and applied the KRDTM for solving three-dimensional equations (1) and (2), where $X = (x, y, z)$, $\mathbf{u} = (u, v, w)$, and $\mathbf{U}_k = (U_k, V_k, W_k)$, and we get

$$\begin{aligned}
(k+1) U_{k+1}(x, y, z) &= -\left(A1_k + B1_k + C1_k \right.\\
&\quad \left. + \frac{\partial P_k(x, y, z)}{\partial x}\right) + \frac{1}{Re}\left(\frac{\partial^2 U_k(x, y, z)}{\partial x^2}\right. \\
&\quad \left. + \frac{\partial^2 U_k(x, y, z)}{\partial y^2} + \frac{\partial^2 U_k(x, y, z)}{\partial z^2}\right),
\end{aligned} \tag{56}$$

$$\begin{aligned}
(k+1) V_{k+1}(x, y, z) &= -\left(A2_k + B2_k + C2_k \right.\\
&\quad \left. + \frac{\partial P_k(x, y, z)}{\partial y}\right) + \frac{1}{Re}\left(\frac{\partial^2 V_k(x, y, z)}{\partial x^2}\right. \\
&\quad \left. + \frac{\partial^2 V_k(x, y, z)}{\partial y^2} + \frac{\partial^2 V_k(x, y, z)}{\partial z^2}\right),
\end{aligned} \tag{57}$$

$$\begin{aligned}
(k+1) W_{k+1}(x, y, z) &= -\left(A3_k + B3_k + C3_k \right.\\
&\quad \left. + \frac{\partial P_k(x, y, z)}{\partial z}\right) + \frac{1}{Re}\left(\frac{\partial^2 W_k(x, y, z)}{\partial x^2}\right. \\
&\quad \left. + \frac{\partial^2 W_k(x, y, z)}{\partial y^2} + \frac{\partial^2 W_k(x, y, z)}{\partial z^2}\right),
\end{aligned} \tag{58}$$

$$\begin{aligned}
(k+1) G_{k+1}(x, y, z) &= -\frac{1}{(Ma)^2}\left(\frac{\partial U_k(x, y)}{\partial x}\right. \\
&\quad \left. + \frac{\partial V_k(x, y)}{\partial y} + \frac{\partial W_k(x, y)}{\partial z}\right) + \frac{1}{Re}\left(\frac{\partial^2 G_k(x, y)}{\partial x^2}\right. \\
&\quad \left. + \frac{\partial^2 G_k(x, y)}{\partial y^2} + \frac{\partial^2 G_k(x, y)}{\partial z^2}\right),
\end{aligned} \tag{59}$$

such that

$$\begin{aligned}
P_k(x, y, z) &= G_k(x, y, z) \\
&\quad + \frac{U_k^2(x, y, z) + V_k^2(x, y, z) + W_k^2(x, y, z)}{2}, \\
A1_k &= \sum_{i=0}^{k} U_i(x, y, z) \frac{\partial U_{k-i}(x, y, z)}{\partial x}, \\
B1_k &= \sum_{i=0}^{k} V_i(x, y, z) \frac{\partial U_{k-i}(x, y, z)}{\partial y}, \\
C1_k &= \sum_{i=0}^{k} W_i(x, y, z) \frac{\partial U_{k-i}(x, y, z)}{\partial z}, \\
A2_k &= \sum_{i=0}^{k} U_i(x, y, z) \frac{\partial V_{k-i}(x, y, z)}{\partial x}, \\
B2_k &= \sum_{i=0}^{k} V_i(x, y, z) \frac{\partial V_{k-i}(x, y, z)}{\partial y}, \\
C2_k &= \sum_{i=0}^{k} W_i(x, y, z) \frac{\partial V_{k-i}(x, y, z)}{\partial z},
\end{aligned}$$

Table 4: The L_2-norm error for u of **P2** at $t = 0.1$ and $Ma = 0.01$.

Grid size	method	Re=20	Re=40	Re=100	Re=500	Max CPUs
11×11	KRDTM	4.34×10^{-7}	5.24×10^{-8}	1.12×10^{-8}	2.30×10^{-9}	0.063
	UCFDM [4]	6.06×10^{-2}	3.26×10^{-2}	2.75×10^{-2}	1.33×10^{-2}	—
21×21	KRDTM	3.42×10^{-7}	4.30×10^{-8}	9.21×10^{-9}	1.90×10^{-9}	0.218
	UCFDM [4]	1.40×10^{-2}	7.37×10^{-3}	3.85×10^{-7}	2.33×10^{-3}	—
41×41	KRDTM	3.02×10^{-7}	4.03×10^{-8}	8.98×10^{-9}	1.87×10^{-9}	0.624
	UCFDM [4]	1.73×10^{-3}	9.48×10^{-4}	5.06×10^{-4}	3.08×10^{-4}	—
81×81	KRDTM	2.83×10^{-7}	3.90×10^{-8}	8.86×10^{-9}	1.86×10^{-9}	2.57
	UCFDM [4]	1.62×10^{-4}	9.56×10^{-5}	5.18×10^{-5}	3.21×10^{-5}	—
161×161	KRDTM	2.74×10^{-7}	3.83×10^{-8}	8.80×10^{-9}	1.85×10^{-9}	10.2
	UCFDM [4]	1.48×10^{-5}	9.60×10^{-6}	5.74×10^{-6}	3.38×10^{-6}	—
321×321	KRDTM	2.69×10^{-7}	3.80×10^{-8}	8.77×10^{-9}	1.85×10^{-9}	41.8
	UCFDM [4]	1.40×10^{-6}	9.59×10^{-7}	6.64×10^{-7}	3.94×10^{-7}	—

Table 5: The L_2-norm error for v of **P2** at $t = 0.1$ and $Ma = 0.01$.

Grid size	Re=20	Re=40	Re=100	Re=500	Max CPUs
11×11	2.54×10^{-7}	2.73×10^{-8}	3.02×10^{-9}	1.30×10^{-10}	0.047
21×21	2.11×10^{-7}	2.46×10^{-8}	2.90×10^{-9}	1.27×10^{-10}	0.172
41×41	1.88×10^{-7}	2.32×10^{-8}	2.83×10^{-9}	1.26×10^{-10}	0.671
81×81	1.77×10^{-7}	2.25×10^{-8}	2.79×10^{-9}	1.25×10^{-10}	2.50
161×161	1.72×10^{-7}	2.22×10^{-8}	2.77×10^{-9}	1.24×10^{-10}	9.80
321×321	1.69×10^{-7}	2.20×10^{-8}	2.76×10^{-9}	1.24×10^{-10}	39.2

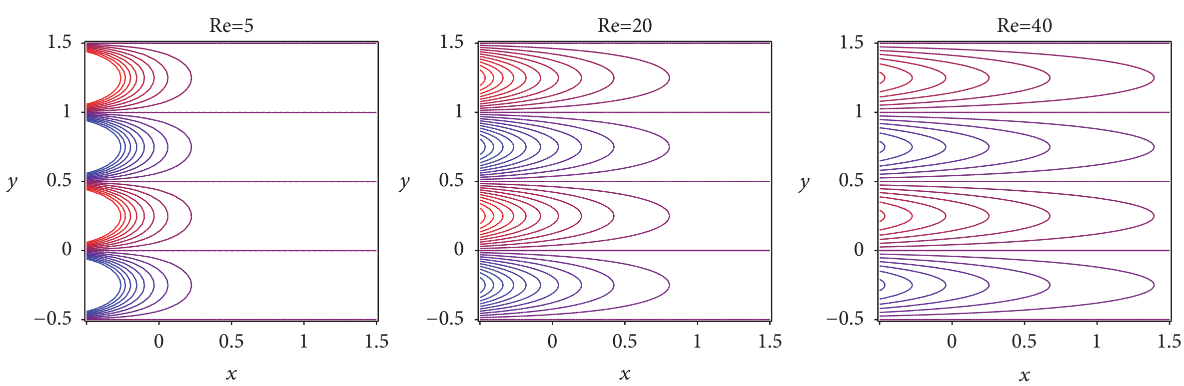

(a) The vorticity Ω

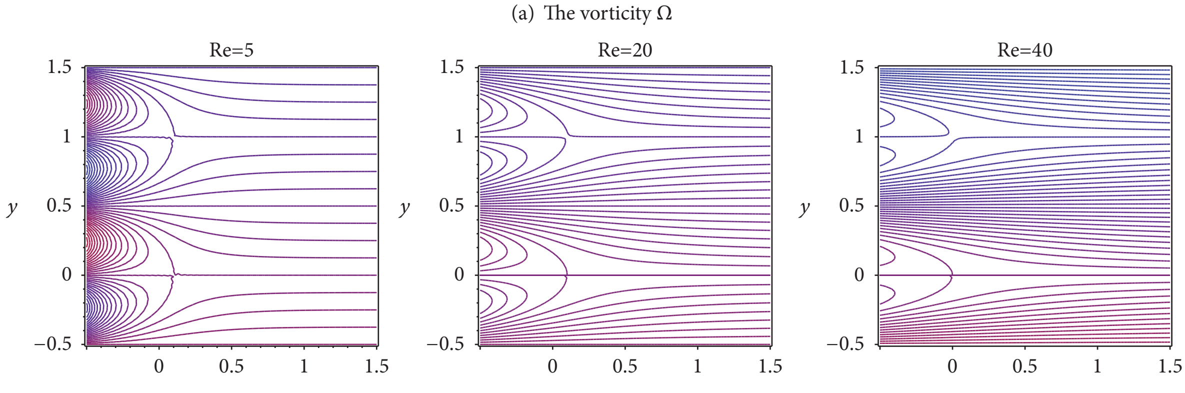

(b) The streamlines ψ

Figure 3: The vorticity and streamlines contour plots for **P2** at $t = 0.1$ and $Ma = 0.01$.

$$
\begin{aligned}
A3_k &= \sum_{i=0}^{k} U_i(x,y,z)\frac{\partial W_{k-i}(x,y,z)}{\partial x},\\
B3_k &= \sum_{i=0}^{k} V_i(x,y,z)\frac{\partial W_{k-i}(x,y,z)}{\partial y},\\
C3_k &= \sum_{i=0}^{k} W_i(x,y,z)\frac{\partial W_{k-i}(x,y,z)}{\partial z},
\end{aligned}
\tag{60}
$$

where $= 0,1,2,3,\ldots$, $U_0(x,y,z) = u(x,y,z,0)$, $V_0(x,y,z) = v(x,y,z,0)$, $W_0(x,y,z) = w(x,y,z,0)$, and $G_0(x,y,z) = g(x,y,z,0)$.

Then the exact solution is obtained as follows:

$$u(x,y,z,\tau) = \lim_{n\to\infty} u_n(x,y,z,\tau), \tag{61}$$

$$v(x,y,z,\tau) = \lim_{n\to\infty} v_n(x,y,z,\tau), \tag{62}$$

$$w(x,y,z,\tau) = \lim_{n\to\infty} w_n(x,y,z,\tau), \tag{63}$$

$$g(x,y,z,\tau) = \lim_{n\to\infty} g_n(x,y,z,\tau), \tag{64}$$

where

$$
\begin{aligned}
u_n(x,y,z,\tau) &= \sum_{k=0}^{n} U_k(x,y,z)\tau^k,\\
v_n(x,y,z,\tau) &= \sum_{k=0}^{n} V_k(x,y,z)\tau^k,\\
w_n(x,y,z,\tau) &= \sum_{k=0}^{n} W_k(x,y,z)\tau^k,\\
g_n(x,y,z,\tau) &= \sum_{k=0}^{n} G_k(x,y,z)\tau^k,
\end{aligned}
\tag{65}
$$

such that

$$
\begin{aligned}
U_1(x,y,z) &= -\frac{3}{Re}\sin(x)\cos(y)\cos(z) - \frac{1}{8}\sin(2x)\\
&\quad\cdot\cos(2z),\\
U_2(x,y,z) &= \frac{9}{2(Re)^2}\sin(x)\cos(y)\cos(z)\\
&\quad - \frac{3}{16Re}(1-\cos(2y))(1+\cos(2z))\sin(2x)\\
&\quad + \sin(x)\sin(y)\cos(z)\left(\frac{3}{2Re}\cos(x)\sin(y)\cos(z)\right.\\
&\quad \left.- \frac{1}{16}\sin(2y)\cos(2z)\right) - \sin(x)\cos(y)\cos(z)\\
&\quad \cdot\left(-\frac{3}{Re}\cos(x)\cos(y)\cos(z)\right.\\
&\quad \left.- \frac{1}{4}\cos(2x)\cos(2z)\right) - \cos(x)\cos(y)\cos(z)\\
&\quad \cdot\left(-\frac{3}{Re}\sin(x)\cos(y)\cos(z)\right.\\
&\quad \left.- \frac{1}{8}\sin(2x)\cos(2z)\right) + \frac{1}{16}(\cos(2x)+\cos(2y))\\
&\quad \cdot\sin(2z)\sin(x)\cos(y)\sin(z) - \frac{1}{2Re}\sin(2x)(1\\
&\quad + 2\cos(2y) + 3\cos(2y)\cos(2z)),\\
&\ \ \vdots,\\
V_1(x,y,z) &= \frac{3}{Re}\cos(x)\sin(y)\cos(z) - \frac{1}{8}\sin(2y)\\
&\quad\cdot\cos(2z),\\
V_2(x,y,z) &= -\frac{9}{2(Re)^2}\cos(x)\sin(y)\cos(z)\\
&\quad - \frac{3}{16Re}(1-\cos(2x))(1+\cos(2z))\sin(2y)\\
&\quad - \sin(x)\sin(y)\cos(z)\\
&\quad \cdot\left(-\frac{3}{2Re}\sin(x)\cos(y)\cos(z)\right.\\
&\quad \left.- \frac{1}{16}\sin(2x)\cos(2z)\right) + \cos(x)\sin(y)\cos(z)\\
&\quad \cdot\left(\frac{3}{Re}\cos(x)\cos(y)\cos(z)\right.\\
&\quad \left.- \frac{1}{4}\cos(2y)\cos(2z)\right) + \cos(x)\cos(y)(\cos(z))\\
&\quad \cdot\left(\frac{3}{Re}\cos(x)\sin(y)\cos(z)\right.\\
&\quad \left.- \frac{1}{8}\sin(2y)\cos(2z)\right) - \frac{1}{16}(\cos(2x)+\cos(2y))\\
&\quad \cdot\sin(2z)\cos(x)\sin(y)\sin(z) - \frac{1}{2Re}\sin(2y)(1\\
&\quad + 2\cos(2x) + 3\cos(2x)\cos(2z)),\\
&\ \ \vdots,\\
W_1(x,y,z) &= \frac{1}{8}(\cos(2x)+\cos(2y))\sin(2z),\\
W_2(x,y,z) &= -\frac{1}{Re}(\cos(2x)+\cos(2y))\sin(2z)\\
&\quad + \frac{1}{2Re}(1-3\cos(2x)\cos(2y))\sin(2z) + \frac{1}{8}\cos(z)\\
&\quad \cdot\sin(2z)(\sin(x)\cos(y)\sin(2x)\\
&\quad - \cos(x)\sin(y)\sin(2y)) - \sin(x)\cos(y)\cos(z)\\
&\quad \cdot\left(\frac{3}{Re}\sin(x)\cos(y)\sin(z) + \frac{1}{4}\sin(2x)\sin(2z)\right)\\
&\quad + \cos(x)\sin(y)\cos(z)\left(-\frac{3}{Re}\cos(x)\sin(y)\sin(z)\right.\\
&\quad \left.+ \frac{1}{4}\sin(2y)\sin(2z)\right),\\
&\ \ \vdots,
\end{aligned}
\tag{66}
$$

and

$$\begin{aligned}
G_1(x,y,z) &= -\frac{1}{2Re}\left[(\cos(2x)+\cos(2y))\right.\\
&\quad\cdot(\cos(2z)+1)+2\cos(2x)\cos(2y)\\
&\quad\left.-(1-3\cos(2x)\cos(2y))\cos(2z)\right],\\
G_2(x,y,z) &= \frac{1}{(Re)^2}\left[\cos(2x)\right.\\
&\quad\cdot(1+\cos(2z)+2\cos(2y)+3\cos(2y)\cos(2z))\\
&\quad+\cos(2y)\\
&\quad\cdot(1+\cos(2z)+2\cos(2x)+3\cos(2x)\cos(2z))\\
&\quad-\cos(2z)\\
&\quad\left.\cdot(1-\cos(2x)-\cos(2y)-3\cos(2x)\cos(2y))\right],\\
&\vdots
\end{aligned} \tag{67}$$

The flow is computed with in a periodic square box defined as $-\pi < x, y, z < \pi$. The condition of the convergence of these solutions is verified by applying Definition 5

$$\begin{aligned}
\gamma_{10} &= \frac{\|U_1(x,y,z)\tau\|}{\|U_0(x,y,z)\|} = \frac{\sqrt{(Re)^2+288\tau}}{4\sqrt{2}Re},\\
\gamma_{20} &= \frac{\|V_1(x,y,z)\tau\|}{\|V_0(x,y,z)\|} = \frac{\sqrt{(Re)^2+288\tau}}{4\sqrt{2}Re},\\
\gamma_{30} &= \frac{\|W_1(x,y,z)\tau\|}{\|W_0(x,y,z)\|} = 0,\\
\gamma_{40} &= \frac{\|G_1(x,y,z)\tau\|}{\|G_0(x,y,z)\|} = \frac{\sqrt{22\tau}}{Re},\\
\gamma_{11} &= \frac{\|U_2(x,y,z)\tau^2\|}{\|U_1(x,y,z)\tau\|}\\
&= \frac{\sqrt{3\left((Re)^4+70(Re)^2+864\right)\tau}}{2\sqrt{(Re)^2+288}Re},\\
\gamma_{21} &= \frac{\|V_2(x,y,z)\tau^2\|}{\|V_1(x,y,z)\tau\|}\\
&= \frac{\sqrt{3\left((Re)^4+70(Re)^2+864\right)\tau}}{2\sqrt{Re^2+288}Re},\\
\gamma_{31} &= \frac{\|W_2(x,y,z)\tau^2\|}{\|W_1(x,y,z)\tau\|} = \frac{\sqrt{(Re)^2+1232\tau}}{Re},\\
\gamma_{41} &= \frac{\|G_2(x,y,z)\tau^2\|}{\|G_1(x,y,z)\tau\|} = \frac{2\sqrt{47\tau}}{\sqrt{11}Re},\\
&\vdots,
\end{aligned} \tag{68}$$

such that $\gamma_0 = \gamma_{10}+\gamma_{20}+\gamma_{30}+\gamma_{40}$, $\gamma_1 = \gamma_{11}+\gamma_{21}+\gamma_{31}+\gamma_{41}, \ldots$. For example, if $Ma = 0.01$, $Re = 100$, and $t = 0.5$, then

$$\begin{aligned}
\gamma_0 &= 0.0020275629 < 1,\\
\gamma_1 &= 0.0100995152 < 1, \ldots,
\end{aligned} \tag{69}$$

if $t = 2$ then

$$\begin{aligned}
\gamma_0 &= 0.0081754148 < 1,\\
\gamma_1 &= 0.0435106065 < 1, \ldots,
\end{aligned} \tag{70}$$

and if $t = 5$ then

$$\begin{aligned}
\gamma_0 &= 0.0204385369 < 1,\\
\gamma_1 &= 0.1087765162 < 1, \ldots
\end{aligned} \tag{71}$$

Tables 6 and 7 show L_2-norm error for u and w with CPU time at time levels $t = 0.5, 2, 5$, $Re = 100$, $Ma = 0.005$, and $Ma = 0.01$. It is clear that the value of the calculated error is acceptable with different time levels; in addition to that the longest period of CPU time for all cases is 1140s. So, we can say that these solutions have a good accuracy and convergence low Mach numbers. The relationship of the change of time with the enstrophy is shown in Figure 4 at $Re = 20, 40, 100, 500$ for $Ma = 0.1, 0.01$. In Figure 5, we explained the change in the contours of the z-component of the vorticity and the velocities with time on the surface $z = 0$ at $Re = 100$ and $Ma = 0.05$.

Fourth problem (P4) is one type of three-dimension Beltrami flow [25, 27, 28], which yield a family of velocity and pressure fields depending on the selection of a and d. In this test, we selected $a = \pi/4$ and $d = \pi/2$. This problem has the exact solution satisfying (1) and (2), which is given by

$$\begin{aligned}
u(x,y,z,t) &= -a\left[\sin(ay+dz)e^{ax}\right.\\
&\quad\left.+\cos(ax+dy)e^{az}\right]e^{-d^2t/Re},\\
v(x,y,z,t) &= -a\left[\sin(az+dx)e^{ay}\right.\\
&\quad\left.+\cos(ay+dz)e^{ax}\right]e^{-d^2t/Re},\\
w(x,y,z,t) &= -a\left[\sin(ax+dy)e^{az}\right.\\
&\quad\left.+\cos(az+dx)e^{ay}\right]e^{-d^2t/Re},\\
p(x,y,z,t) &= -\frac{a^2}{2}\left[e^{2ax}+e^{2ay}+e^{2az}\right.\\
&\quad+2\sin(ax+dy)\cos(az+dx)e^{a(y+z)}\\
&\quad+2\sin(ay+dz)\cos(ax+dy)e^{a(z+x)}\\
&\quad\left.+2\sin(az+dx)\cos(ay+dz)e^{a(x+y)}\right]e^{-2d^2t/Re},
\end{aligned} \tag{72}$$

and when we applied KRDTM for solving (1) and (2), we get the same solutions in (61), (62), (63), and (64) with

$$\begin{aligned}
U_1(x,y,z) &= \frac{ad^2}{Re}\left(\sin(ay+dz)e^{ax}+\cos(ax+dy)\right.\\
&\quad\left.\cdot e^{az}\right),\\
U_2(x,y,z) &= -\frac{ad^4}{2(Re)^2}\left(\sin(ay+dz)e^{ax}+\cos(ax\right.\\
&\quad\left.+dy)e^{az}\right)-\frac{2a}{Re}\left[e^{a(x+y)}\left(a^2\left(\left(a^2-d^2\right)\right.\right.\right.
\end{aligned}$$

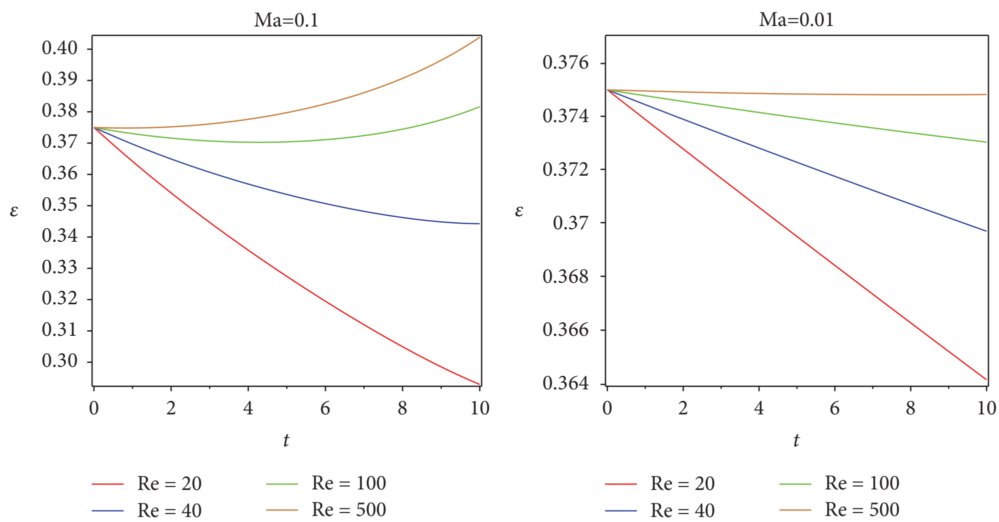

FIGURE 4: The enstrophy for **P3**.

$$
\begin{aligned}
&\cdot \sin(ay+dz) + d^2\cos(ay+dz)) \sin(az+dx) \\
&+ a^3 d (2\sin(ay+dz) - \cos(ay+dz)) \\
&\cdot \cos(az+dx)) + e^{a(y+z)} (((a^2+d^2) \\
&\cdot \cos(ax+dy) - ad\sin(ax+dy)) a^2 \\
&\cdot \sin(az+dx) + (a^2 d^2 \cos(ax+dy) + 2a^3 d \\
&\cdot \sin(ax+dy)) \cos(az+dx)) + e^{a(z+x)} ((a^4 \\
&\cdot \cos(ax+dy) + a^4 \sin(ax+dy)) \sin(ay+dz) \\
&+ 2a^3 d \sin(ax+dy)\cos(ay+dz)) \\
&- 2a^2 e^{2ax}\left(a^2 + \frac{d^2}{2}\right)\Bigg],
\end{aligned}
$$

$$\vdots,$$

$$
\begin{aligned}
V_1(x,y,z) &= \frac{ad^2}{Re}(\sin(az+dx)e^{ay} + \cos(ay+dz) \\
&\quad \cdot e^{ax}), \\
V_2(x,y,z) &= -\frac{ad^4}{2(Re)^2}(\sin(az+dx)e^{ay} + \cos(ay \\
&\quad + dz)e^{ax}) - \frac{2a}{Re}\Bigg[e^{a(y+z)}(a^2((a^2-d^2) \\
&\quad \cdot \sin(az+dx) + d^2\cos(az+dx)) \sin(ax+dy) \\
&\quad + a^3 d(2\sin(az+dx) - \cos(az+dx)) \\
&\quad \cdot \cos(ax+dy)) + e^{a(z+x)}(a^2((a^2+d^2) \\
&\quad \cdot \cos(ay+dz) - ad\sin(ay+dz)) \sin(ax+dy) \\
&\quad + (d^2 a^2 \cos(ay+dz) + 2a^3 d\sin(ay+dz)) \\
&\quad \cdot \cos(ax+dy)) \\
&\quad + e^{a(x+y)}(a^4(\cos(ay+dz) + \sin(ay+dz)) \\
&\quad \cdot \sin(az+dx)) + 2a^3 d\sin(ay+dz) \\
&\quad \cdot \cos(az+dx)) - 2a^2 e^{2ay}\left(a^2 + \frac{d^2}{2}\right)\Bigg], \\
W_1(x,y,z) &= \frac{ad^2}{Re}(\sin(ax+dy)e^{az} + \cos(az+dx) \\
&\quad \cdot e^{ay}), \\
W_2(x,y,z) &= -\frac{ad^4}{2(Re)^2}(\sin(ax+dy)e^{az} + \cos(az \\
&\quad + dx)e^{ay}) - \frac{2a}{Re}\Bigg[e^{a(y+z)}(a^4(\sin(az+dx) \\
&\quad + \cos(az+dx)) \sin(ax+dy) + 2a^3 d \\
&\quad \cdot \cos(ax+dy)\sin(az+dx)) \\
&\quad + e^{a(z+x)}((a^2(a^2-d^2)\sin(ay+dz) + 2a^3 d \\
&\quad \cdot \cos(ay+dz)) \sin(ax+dy) + (a^2 d^2 \\
&\quad \cdot \sin(ay+dz) - ad\cos(ay+dz)) \cos(ax+dy)) \\
&\quad + e^{a(x+y)}(a^2((a^2+d^2)\cos(az+dx) - ad \\
&\quad \cdot \sin(az+dx)) \sin(ay+dz) + (a^2 d^2 \\
&\quad \cdot \cos(az+dx) + 2ad\sin(az+dx)) \\
&\quad \cdot \cos(ay+dz)) - 2a^2 e^{2az}\left(a^2 + \frac{d^2}{2}\right)\Bigg],
\end{aligned}
$$

$$\vdots, \tag{73}$$

and

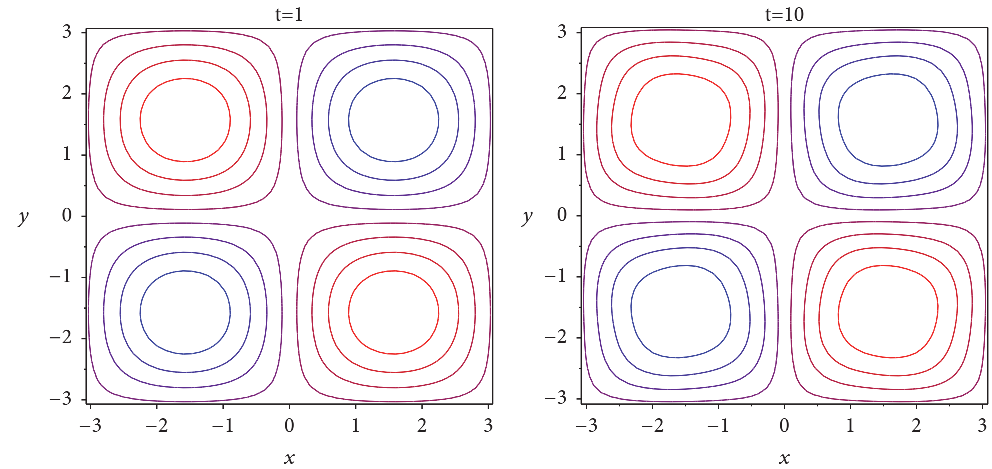

(a) z-component of vorticity Ω

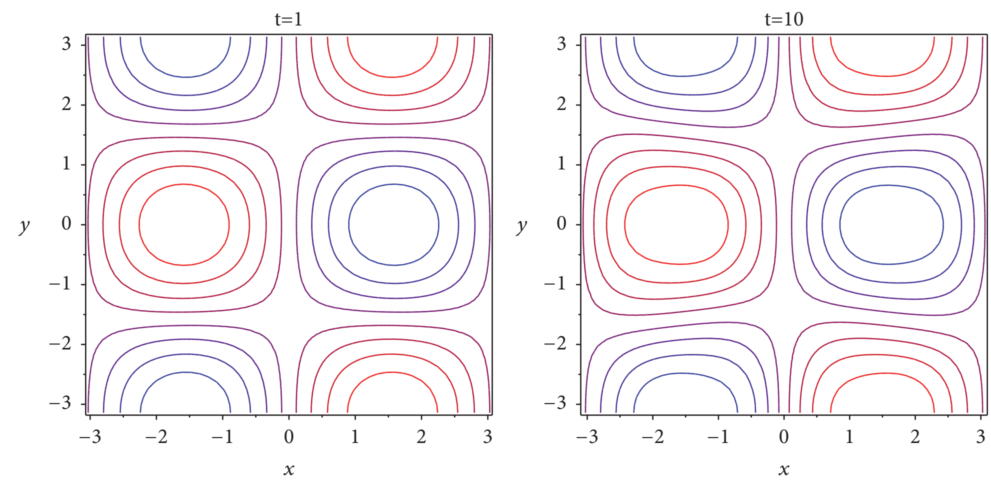

(b) u velocity component

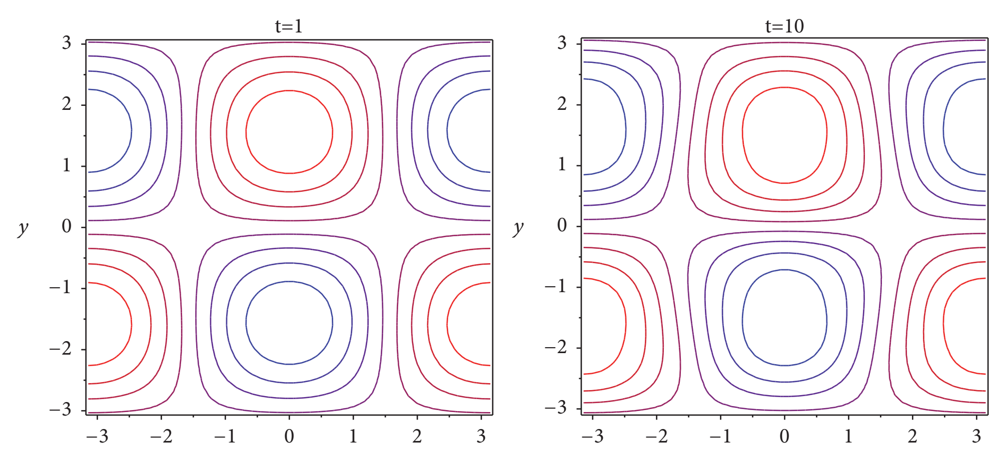

(c) v velocity component

FIGURE 5: The Contours plots of z-component of vorticity, u and v velocity components for **P3** on $z = 0$ at $Re = 100$ and $Ma = 0.05$.

$$G_1(x,y,z) = \frac{4a^2}{Re}\left[e^{a(x+y)}\left(-ad\left(\cos(ay+dz)-\sin(ay+dz)\right)\cos(az+dx)+\left(a^2\sin(ay+dz)+d^2\cos(ay+dz)\right)\right.\right.$$
$$\cdot\sin(az+dx)\Big)+e^{a(y+z)}\left(-ad\left(\cos(az+dx)-\sin(az+dx)\right)\cos(ax+dy)+\left(a^2\sin(az+dx)+d^2\cos(az+dx)\right)\right.$$
$$\cdot\sin(ax+dy)\Big)+e^{a(z+x)}\left(-\left(ad\cos(ay+dz)-d^2\sin(ay+dz)\right)\cos(ax+dy)+\left(a^2\sin(ay+dz)\right.\right.$$
$$\left.\left.\left.+ad\cos(ay+dz)\right)\sin(ax+dy)\right)-a^2\left(e^{2ax}+e^{2ay}+e^{2az}\right)\right],$$

$$G_2(x,y,z) = \frac{4a^2}{(Re)^2}\left[\left(e^{a(y+z)}\left(2ad\left(\left(a^2+d^2\right)\cos(az+dx)+\left(a^2-d^2\right)\sin(az+dx)\right)\cos(ax+dy)\right.\right.\right. \tag{74}$$
$$+\left(\left(a^4-d^4\right)\cos(az+dx)-4a^2d^2\sin(az+dx)\right)\sin(ax+dy)\Big)$$
$$+e^{a(z+x)}\left(2ad\left(\left(a^2+d^2\right)\cos(ay+dz)+\left(a^4-d^4\right)\sin(ay+dz)\right)\right)\times\cos(ax+dy)+\left(2ad\left(a^2-d^2\right)\cos(ay+dz)\right.$$
$$\left.-4a^2d^2\sin(ay+dz)\right)\sin(ax+dy)\Big)+e^{a(x+y)}\left(2ad\left(\left(a^2+d^2\right)\cos(ay+dz)+\left(a^2-d^2\right)\sin(ay+dz)\right)\right.$$
$$\left.\left.\times\cos(az+dx)+\left(\left(a^4-d^4\right)\cos(ay+dz)-4a^2d^2\sin(ay+dz)\right)\sin(az+dx)\right)+a^2\left(e^{2ax}+e^{2ay}+e^{2az}\right)\right],$$
$$\vdots$$

These solutions satisfy the conditions of convergence at the domain $[-1,1]^3$,

$$\gamma_{10} = \frac{\|U_1(x,y,z)\,\tau\|}{\|U_0(x,y,z)\|} = \frac{2.4674011\tau}{Re},$$
$$\gamma_{20} = \frac{\|V_1(x,y,z)\,\tau\|}{\|V_0(x,y,z)\|} = \frac{2.4674011\tau}{Re},$$
$$\gamma_{30} = \frac{\|W_1(x,y,z)\,\tau\|}{\|W_0(x,y,z)\|} = \frac{2.4674011\tau}{Re},$$
$$\gamma_{40} = \frac{\|G_1(x,y,z)\,\tau\|}{\|G_0(x,y,z)\|} = \frac{2.917691460\tau}{Re},$$
$$\gamma_{11} = \frac{\|U_2(x,y,z)\,\tau^2\|}{\|U_1(x,y,z)\,\tau\|} = \frac{3.0495132689\sqrt{(Re)^2-0.020148681Re+0.1636659976\tau}}{Re},$$
$$\gamma_{21} = \frac{\|V_2(x,y,z)\,\tau^2\|}{\|V_1(x,y,z)\,\tau\|} = \frac{3.0495132689\sqrt{(Re)^2-0.020148681Re+0.1636659976\tau}}{Re}, \tag{75}$$
$$\gamma_{31} = \frac{\|W_2(x,y,z)\,\tau^2\|}{\|W_1(x,y,z)\,\tau\|} = \frac{3.0495132689\sqrt{(Re)^2-0.020148681Re+0.1636659976\tau}}{Re},$$
$$\gamma_{41} = \frac{\|G_2(x,y,z)\,\tau^2\|}{\|G_1(x,y,z)\,\tau\|} = \frac{4.3109179800\tau}{Re},$$
$$\vdots,$$

such that $\gamma_0 = \gamma_{10}+\gamma_{20}+\gamma_{30}+\gamma_{40}$, $\gamma_1 = \gamma_{11}+\gamma_{21}+\gamma_{31}+\gamma_{41},\ldots$.

For example, if $Ma = 0.01$, $Re = 100$, and $t = 2$, then

$$\gamma_0 = 0.2063978953\times10^{-2} < 1, \quad \gamma_1 = 0.1838160431 < 1,\ldots, \tag{76}$$

if $t = 5$ then

$$\gamma_0 = 0.5159947383\times10^{-2} < 1, \quad \gamma_1 = 0.4595401079 < 1,\ldots, \tag{77}$$

if $Re = 1600$ and $t = 2$ then

$$\gamma_0 = 0.1289986845\times10^{-3} < 1, \quad \gamma_1 = 0.1830235364 < 1,\ldots, \tag{78}$$

and if $t = 5$ then

$$\gamma_0 = 0.3224967113\times10^{-3} < 1, \quad \gamma_1 = 0.4575588408 < 1,\ldots \tag{79}$$

The L_2-norm error for the u velocity component with CPU time is calculated in Table 8 to study the accuracy of these approximate solutions; the results show an excellent accuracy of our method for all values of Reynolds number at $t = 0.5, 2, 5$ and $Ma = 0.01$, with good implementation period ranging between $2.09s$, $1080s$. The computed enstrophy is compared with their exact values in the same period of time in Figure 6 at $Re = 100, 1600$ for two Mach numbers. In Figure 7, we explained the z−component of the computed vorticity on surface $z = 0$ at $Re = 100$ and $t = 5$ in two domains $[-1,1]^2$ and $[-5,5]^2$. Through these figures, we could notice the relationship between the accuracy of these approximate solutions and Mach numbers which is with decreasing Mach number.

TABLE 6: The L_2-norm errors for u and w of **P3** at $Re = 100$ and $Ma = 0.005$.

Grid size	t=0.5	t=2	t=5	Max CPUs
u velocity				
$33 \times 33 \times 33$	1.82×10^{-8}	1.17×10^{-6}	1.82×10^{-5}	2.12
$65 \times 65 \times 65$	1.73×10^{-8}	1.11×10^{-6}	1.73×10^{-5}	18.4
$129 \times 129 \times 129$	1.69×10^{-8}	1.08×10^{-6}	1.69×10^{-5}	126
$257 \times 257 \times 257$	1.67×10^{-8}	1.07×10^{-6}	1.67×10^{-5}	995
w velocity				
$33 \times 33 \times 33$	1.21×10^{-8}	7.74×10^{-7}	1.21×10^{-5}	2.42
$65 \times 65 \times 65$	1.19×10^{-8}	7.60×10^{-7}	1.19×10^{-5}	18.4
$129 \times 129 \times 129$	1.18×10^{-8}	7.52×10^{-7}	1.18×10^{-5}	143
$257 \times 257 \times 257$	1.17×10^{-8}	7.49×10^{-7}	1.17×10^{-5}	1120

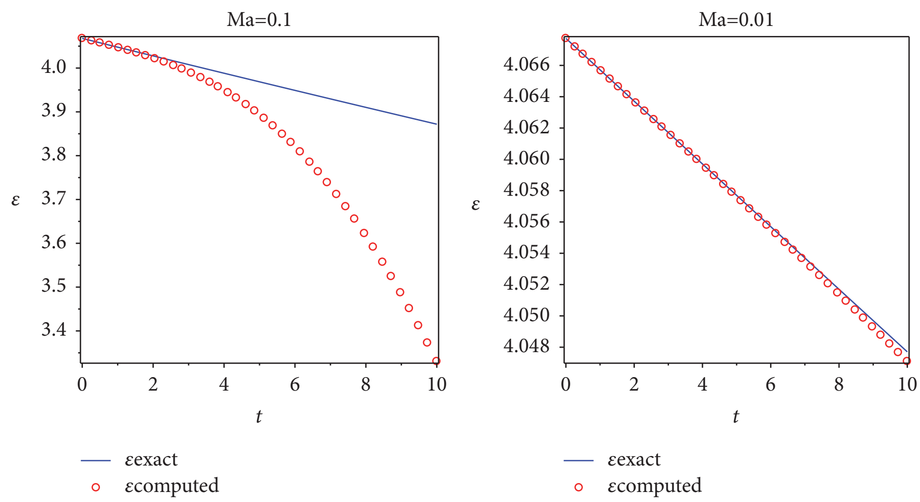

(a) Re=100

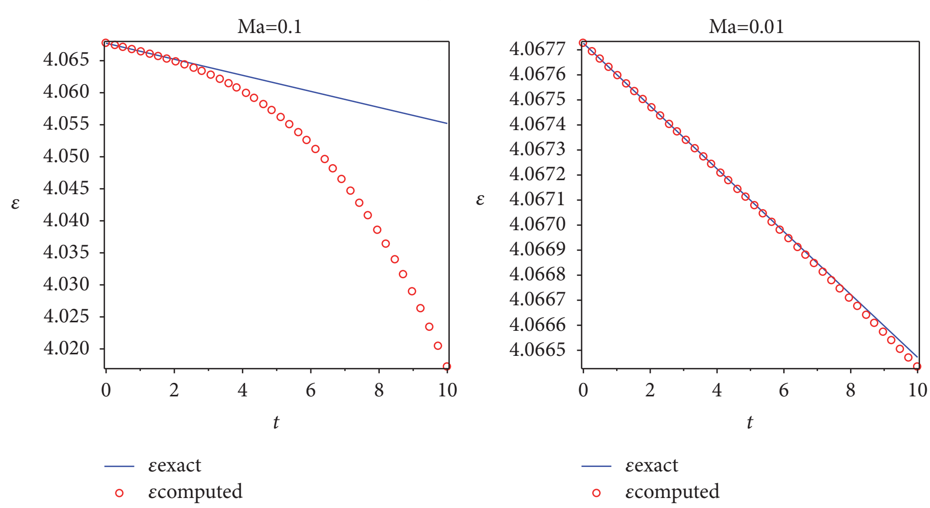

(b) Re=1600

FIGURE 6: The enstrophy for **P4**.

5. Conclusions

In this paper, the simulations of two- and three-dimensional unsteady viscous incompressible flow problems are presented by using the kinetically reduced local Navier-Stokes equations with the reduced differential transform method. New approximate analytical solutions obtained by KRDTM are tested in terms of accuracy and convergence. The results show that the new solutions have good accuracy and convergence, especially with high Reynolds numbers and low Mach numbers. The comparison explained that the computational time of these solutions is faster than that of other numerical

Table 7: The L_2-norm errors for u and w of **P3** at $Re = 100$ and $Ma = 0.01$.

Grid size	t=0.5	t=2	t=5	Max CPUs
u velocity				
$33 \times 33 \times 33$	1.46×10^{-7}	9.32×10^{-6}	1.46×10^{-4}	2.22
$65 \times 65 \times 65$	1.39×10^{-7}	8.87×10^{-6}	1.39×10^{-4}	17.7
$129 \times 129 \times 129$	1.35×10^{-7}	8.65×10^{-6}	1.35×10^{-4}	128
$257 \times 257 \times 257$	1.33×10^{-7}	8.53×10^{-6}	1.33×10^{-4}	1000
w velocity				
$33 \times 33 \times 33$	9.68×10^{-8}	6.19×10^{-6}	9.68×10^{-5}	2.47
$65 \times 65 \times 65$	9.50×10^{-8}	6.08×10^{-6}	9.50×10^{-5}	18.5
$129 \times 129 \times 129$	9.40×10^{-8}	6.02×10^{-6}	9.40×10^{-5}	144
$257 \times 257 \times 257$	9.36×10^{-8}	5.99×10^{-6}	9.36×10^{-5}	1140

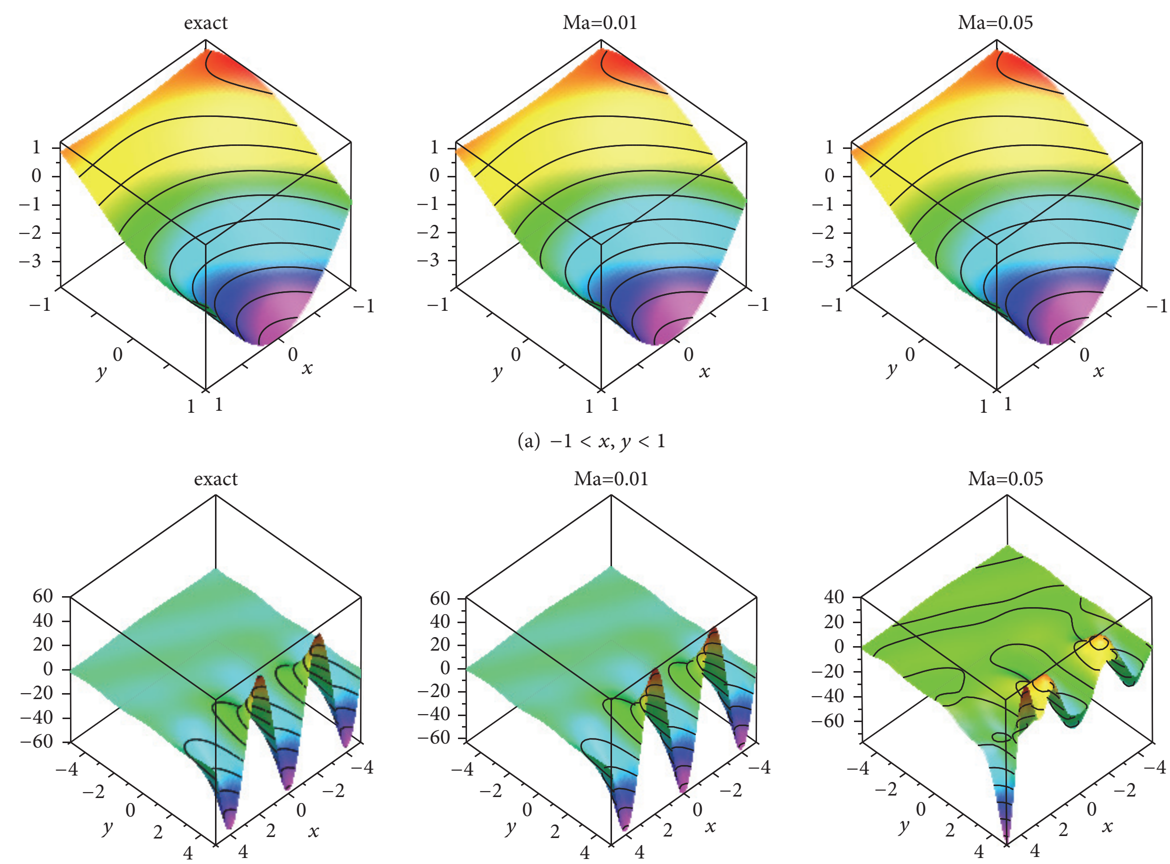

(a) $-1 < x, y < 1$

(b) $-5 < x, y < 5$

Figure 7: The surface plots of the z-component of the computed vorticity for **P4** on $z = 0$ at $Re = 100$ and $t = 5$.

solutions. Therefore, KRDTM is an effective and accurate method for solving the unsteady viscous incompressible flow problems.

Data Availability

The data used to support the findings of this study are included within the article.

Conflicts of Interest

The authors declare that they have no conflicts of interest.

Acknowledgments

We would like to thank the English proofreader Assistant Professor Mahdi Mohsin Mohammed for his careful reading.

Table 8: The L_2-norm errors for u of **P4** at $Ma = 0.01$.

Grid size	t=0.5	t=2	t=5	Max CPUs
$Re = 100$				
$33 \times 33 \times 33$	6.18×10^{-6}	1.00×10^{-4}	6.44×10^{-4}	2.44
$65 \times 65 \times 65$	5.89×10^{-6}	9.54×10^{-5}	6.15×10^{-4}	20.4
$129 \times 129 \times 129$	5.74×10^{-6}	9.31×10^{-5}	6.00×10^{-4}	151
$257 \times 257 \times 257$	5.67×10^{-6}	9.19×10^{-5}	5.93×10^{-4}	1080
$Re = 500$				
$33 \times 33 \times 33$	1.24×10^{-6}	2.00×10^{-5}	1.29×10^{-4}	2.9
$65 \times 65 \times 65$	1.18×10^{-6}	1.91×10^{-5}	1.23×10^{-4}	15.9
$129 \times 129 \times 129$	1.15×10^{-6}	1.86×10^{-5}	1.20×10^{-4}	127
$257 \times 257 \times 257$	1.13×10^{-6}	1.84×10^{-5}	1.19×10^{-4}	996
$Re = 1600$				
$33 \times 33 \times 33$	3.86×10^{-7}	6.26×10^{-6}	4.03×10^{-5}	2.20
$65 \times 65 \times 65$	3.68×10^{-7}	5.96×10^{-6}	3.84×10^{-5}	16.8
$129 \times 129 \times 129$	3.59×10^{-7}	5.82×10^{-6}	3.75×10^{-5}	130
$257 \times 257 \times 257$	3.54×10^{-7}	5.75×10^{-6}	3.71×10^{-5}	1020

References

[1] S. Ansumali, I. V. Karlin, and H. C. Öttinger, "Thermodynamic theory of incompressible hydrodynamics," *Physical Review Letters*, vol. 94, no. 8, 2005.

[2] I. V. Karlin, A. G. Tomboulides, C. E. Frouzakis, and S. Ansumali, "Kinetically reduced local Navier-Stokes equations: An alternative approach to hydrodynamics," *Physical Review E: Statistical, Nonlinear, and Soft Matter Physics*, vol. 74, no. 3, 2006.

[3] S. Borok, S. Ansumali, and I. V. Karlin, "Kinetically reduced local Navier-Stokes equations for simulation of incompressible viscous flows," *Physical Review E: Statistical, Nonlinear, and Soft Matter Physics*, vol. 76, no. 6, 2007.

[4] A. Shah, L. Yuan, and A. Khan, "Upwind compact finite difference scheme for time-accurate solution of the incompressible Navier-Stokes equations," *Applied Mathematics and Computation*, vol. 215, no. 9, pp. 3201–3213, 2010.

[5] T. Hashimoto, I. Tanno, Y. Tanaka, K. Morinishi, and N. Satofuka, "Simulation of decaying two-dimensional turbulence using kinetically reduced local Navier-Stokes equations," in *Proceedings of the Seventh International Conference on Computational Fluid Dynamics*, vol. 88, pp. 715–718, 2012.

[6] T. Hashimoto, I. Tanno, Y. Tanaka, K. Morinishi, and N. Satofuka, "Higher order numerical simulation of unsteady viscous incompressible flows using kinetically reduced local Navier-Stokes equations on a GPU," *Computers and Fluids*, vol. 110, pp. 108–113, 2015.

[7] A. S. J. Al-Saif, "Analytical approximate solutions for two-dimensional incompressible Navier-Stokes equations," *Advances in Physics Theories and Applications*, vol. 49, pp. 69–86, 2015.

[8] A. Shah, H. Fayyaz, and M. Rizwan, "Fourth-order central compact scheme for the numerical solution of incompressible Navier-Stokes equations," *International Journal of Computer Mathematics*, vol. 94, no. 12, pp. 2492–2507, 2017.

[9] J. K. Zhou, *Differential transformation and its application for electrical circuits*, Huazhong University Press, Wuhan, China, 1986.

[10] Y. Keskin and G. Oturanc, "Reduced differential transform method for partial differential equations," *International Journal of Nonlinear Sciences and Numerical Simulation*, vol. 10, no. 6, pp. 7414–7749, 2009.

[11] Y. Keskin and G. Oturanc, "Reduced differential transform method for generalized KdV equations," *Mathematical & Computational Applications*, vol. 15, no. 3, pp. 382–393, 2010.

[12] P. K. Gupta, "Approximate analytical solutions of fractional Benney-Lin equation by reduced differential transform method and the homotopy perturbation method," *Computers & Mathematics with Applications*, vol. 61, no. 9, pp. 2829–2842, 2011.

[13] R. Abazari and M. Abazari, "Numerical simulation of generalized Hirota-Satsuma coupled KdV equation by RDTM and comparison with DTM," *Communications in Nonlinear Science and Numerical Simulation*, vol. 17, no. 2, pp. 619–629, 2012.

[14] M. Rawashdeh, "Using the Reduced Differential Transform Method to solve nonlinear PDEs Arises in biology and physics," *World Applied Sciences Journal*, vol. 23, no. 8, pp. 1037–1043, 2013.

[15] B. Benhammouda, H. Vazquez-Leal, and A. Sarmiento-Reyes, "Modified Reduced Differential Transform Method for Partial Differential-Algebraic Equations," *Journal of Applied Mathematics*, vol. 2014, Article ID 279481, 9 pages, 2014.

[16] B. C. Neog, "Solutions of some system of non-linear PDEs using reduced differential transform method," *IOSR Journal of Mathematics*, vol. 11, pp. 37–44, 2015.

[17] K. Wang and S. Liu, "Analytical study of time-fractional Navier-Stokes equation by using transform methods," *Advances in Difference Equations*, Paper No. 61, 12 pages, 2016.

[18] J. Yu, J. Jing, Y. Sun, and S. Wu, "(n+1) dimensional reduced differential transform method for solving partial differential equations," *Applied Mathematics and Computation*, vol. 273, pp. 697–705, 2016.

[19] M. S. Mohamed and K. A. Gepreel, "Reduced differential transform method for nonlinear integral member of Kadomtsev-Petviashvili hierarchy differential equations," *Journal of the Egyptian Mathematical Society*, vol. 25, no. 1, pp. 1–7, 2017.

[20] E. A. Az-Zobi and K. Al-Khaled, "A new convergence proof of the Adomian decomposition method for a mixed hyperbolic

elliptic system of conservation laws," *Applied Mathematics and Computation*, vol. 217, no. 8, pp. 4248–4256, 2010.

[21] H. Saberi Nik and F. Soleymani, "A taylor-type numerical method for solving nonlinear ordinary differential equations," *Alexandria Engineering Journal*, vol. 52, no. 3, pp. 543–550, 2013.

[22] G. I. Taylor and A. E. Green, "Mechanism of the production of small eddies from large ones," *Proceedings of the Royal Society A Mathematical, Physical and Engineering Sciences*, vol. 158, no. 895, pp. 499–521, 1937.

[23] M. E. Brachet, D. I. Meiron, B. G. Nickel, R. H. Morf, U. Frisch, and S. A. Orszag, "Small-scale structure of the taylor-green vortex," *Journal of Fluid Mechanics*, vol. 130, pp. 411–452, 1983.

[24] W. M. van Rees, A. Leonard, D. I. Pullin, and P. Koumoutsakos, "A comparison of vortex and pseudo-spectral methods for the simulation of periodic vortical flows at high Reynolds numbers," *Journal of Computational Physics*, vol. 230, no. 8, pp. 2794–2805, 2011.

[25] M. Piatkowski, S. Müthing, and P. Bastian, "A stable and high-order accurate discontinuous Galerkin based splitting method for the incompressible Navier-Stokes equations," *Journal of Computational Physics*, vol. 356, pp. 220–239, 2018.

[26] Y. Bo, P. Wang, Z. Guo, and L.-P. Wang, "DUGKS simulations of three-dimensional Taylor-Green vortex flow and turbulent channel flow," *Computers & Fluids*, pp. 1–13, 2017.

[27] C. R. Ethier and D. A. Steinman, "Exact fully 3D Navier–Stokes solutions for benchmarking," *International Journal for Numerical Methods in Fluids*, vol. 19, no. 5, pp. 369–375, 1994.

[28] L. Botti and D. A. Di Pietro, "A pressure-correction scheme for convection-dominated incompressible flows with discontinuous velocity and continuous pressure," *Journal of Computational Physics*, vol. 230, no. 3, pp. 572–585, 2011.